ROLE OF TIP CLEARANCE FLOW ON AXIAL COMPRESSOR STABILITY

by

HUU DUC VO

B.Eng., Mechanical Engineering, McGill University, 1994
S.M., Aeronautics and Astronautics, Massachusetts Institute of Technology, 1997

Submitted to the Department of Aeronautics and Astronautics
in partial fulfillment of the requirements for the degree of

Doctor of Philosophy

at the

Massachusetts Institute Of Technology

September 2001
[February 2002]

Author: _____
Department of Aeronautics and Astronautics
September 18, 2001

Certified by: _____
Choon S. Tan, Ph.D.
Senior Research Engineer
Thesis Supervisor

Certified by: _____
Edward M. Greitzer, Ph.D.
H. Nelson Slater Professor of Aeronautics and Astronautics
Thesis Supervisor

Certified by: _____
Eugene E. Covert, Ph.D.
T. Wilson Professor Emeritus of Aeronautics and Astronautics

Accepted by: _____
Wallace E. VanderVelde, Sc.D.
Professor of Aeronautics and Astronautics
Chair, Committee on Graduate Students

ROLE OF TIP CLEARANCE FLOW ON AXIAL COMPRESSOR STABILITY

By

Huu Duc Vo

Abstract

An examination of the fluid dynamic phenomena that link tip clearance flow to the formation of short length-scale (spike) rotating stall disturbances has been carried out. It is found that the onset of growth in tip clearance blockage characterizes the lowest flow coefficient for which a steady blade passage solution exists. It is also found that this condition leads to the formation of spike disturbances. A scenario and criteria for this tip clearance blockage behavior are proposed based on trailing edge backflow and leading edge spillage to the adjacent blade passage. Both are associated with tip clearance flow and occur below the blade tip. Trailing edge backflow involves tip clearance fluid from adjacent blade passages. The leading edge spillage consists of tip clearance fluid from the local blade passage. These two criteria explain the observed length-scale of spike disturbances. This scenario is consistent with several experimental observations on axial compressor stall inception. The implications of these results on the role of single blade passage computations in stall prediction and on the effectiveness of techniques used to delay stall are also discussed.

Acknowledgements

Many people have given me great assistance in this project and have made my experience at M.I.T. more enjoyable. I would like to extend my deep gratitude to them.

First, I would like to thank my thesis advisors, Dr. C. S. Tan and Professor E.M. Greitzer, for their support and guidance throughout this project. Much gratitude is also extended to Professor W.N. Dawes, Dr. J. R. Wood, Professor J. D. Denton and Dr. L. Xu who provided me with the numerical tools and support for the numerical computations and analysis essential to this project. I would also like to thank Dr. M. D. Hathaway, Dr. J. J. Adamczyk , Dr. A. J. Strazisar, Dr. D. E. Van Zante, Dr. C. Hah, Dr. J. Rhie, Mr. J. Bleeg and Dr. H. Saathoff for providing me the data for other compressor geometries with which to compare my results. I also owe many thanks for technical advice and insightful comments from Professor E. E. Covert, Professor F. E. Marble, Professor N.A. Cumpsty, Dr. T. P. Hynes, Dr. I. J. Day and Dr. J. P. Longley and Professor J. J. Deyst on the several occasions when I had the privilege to discuss my research with them.

In addition, I am also thankful to the staff and students of the M.I.T. Gas Turbine Laboratory, in particular Dr. Y. Gong, Borislav Sirakov, Taek Choi, Dr. J. Bae, Dongwon Choi, Hyung-Soo Moon, Jinwook Lee, Anthony Chobot and Dr. A. Merchant, who are both supportive friends and colleagues with whom I regularly carried out technical discussion on my research, and Paul Warren, Holly Anderson, Mary McDavitt and Diana Park for their help with all the technical equipment acquisitions, setup and repairs needed to do my research. I also have much appreciation for the supporting staff of the Aeroshark computer cluster at the NASA Glenn Research Center. This cluster was used for most of the computations carried out in this project.

Last but not least, I would like to thank my family, particularly my parents for their continued moral and logistical support throughout all the years that I have spent at M.I.T., as well as the Luu family for their friendship and help.

This work was funded by the U.S. Air Force Office of Scientific Research under Grant F49620-00-1-0014 monitored by Dr. T. J. Beutner, whose support is gratefully acknowledged.

Table of Contents

Abstract 3

Acknowledgements 5

Table of Contents 7

List of Figures and Tables 11

Chapter 1: Introduction 15

1.1 Background..... 15

1.2 Problem Definition and Research Questions..... 19

1.3 Research Objectives..... 21

1.4 Approach..... 21

1.5 Thesis Organization..... 23

1.6 Contributions..... 23

Chapter 2: Generic Passage Flow Features Associated with Spike Stall Inception 25

2.1 Pertinent Flow Characteristics..... 25

2.2 Low-Speed Compressor Rotor..... 28

2.2.1 Spike Stall Inception..... 29

2.2.2 Modal Stall Inception..... 32

2.3 High-Speed Compressor Data..... 32

2.3.1 Spike Stall Inception..... 33

2.3.2 Modal Stall Inception..... 33

2.4 Summary..... 36

Chapter 3: Blade Passage Equilibrium Flow Limit 37
3.1 Single Blade Passage Computations..... 37
3.2 Cause of Equilibrium Flow Limit..... 40
3.2.1 Tip Clearance Flow Behavior..... 40
3.2.2 Threshold Flow Events..... 43
3.2.3 Trailing Edge Backflow Below Blade Tip..... 45
3.2.4 Leading Edge spillage Below Blade Tip..... 48
3.2.5 Criteria for Blade Passage Equilibrium Flow Limit..... 50
3.3 Summary..... 53

Chapter 4: Link to Stall Inception 55
4.1 Formation of Spike Disturbances..... 55
4.2 Consistency with Stall Inception Experiments..... 61
4.2.1 Optimal Measurement Location for Spike Disturbances..... 61
4.2.2 Critical Incidence Theory..... 62
4.2.3 Change of Stall Inception Type With Tip Clearance Size..... 65
4.2.4 Effectiveness of stall Margin Improvements Strategies..... 66
4.3 Summary..... 68

Chapter 5: Summary, Conclusions and Recommendations for Future Work 69
5.1 Summary..... 69
5.2 Conclusions..... 69
5.3 Implications..... 71
5.4 Recommendations for Future Work..... 72

Bibliography 75

Appendix A: Assessment Vortex Kinematics Stall Criteria 79

Appendix B: Steady-State Computations 81
B.1 Numerical Code..... 81

B.2 Mesh..... 82
B.3 Computational Procedure..... 84

Appendix C: Unsteady (Time-Accurate) Computations **87**
C.1 Numerical Code..... 87
C.2 Mesh..... 88
C.3 Computational Procedure..... 89

Appendix D: Flow Oscillations at Large Tip Clearances **93**

List of Figures and Tables

Figures

1.1 Compressor stability limit..... 15
1.2 Rotating stall..... 16
1.3 Effects of rotating stall on compressor performance..... 16
1.4 Modal stall inception and associated hot-wire (axial velocity) trace..... 17
1.5 Spike stall inception and associated hot-wire (axial velocity) trace..... 17
1.6 Problem definition in context of rotating stall..... 19
1.7 Potential of single blade passage computation in stall prediction..... 20

2.1 Blade boundary layer below blade tip..... 26
2.2 Basic features of tip clearance flow..... 27
2.3 Interface between the incoming flow and tip clearance flow..... 28
2.4 E3 rotor B steady single blade passage computations at 1.2% chord tip clearance..... 30
2.5 E3 rotor B steady single blade passage computations at 3.0% chord tip clearance..... 31
2.6 Rotor 35 steady single blade passage computations (NASA) with inlet stagnation pressure distortion..... 34
2.7 Rotor 37 steady single blade passage computations (Pratt & Whitney) without inlet stagnation pressure distortion..... 35
2.8 Rotor casing oil flow pattern near stall on a low-speed single-stage compressor exhibiting spike stall inception [24]..... 36

3.1 Improvement in E3 rotor B mesh for time-accurate computations..... 38
3.2 Stagnation-to-static pressure rise characteristic across E3 rotor at different tip clearances from time –accurate single blade passage computations..... 39
3.3 Single blade passage stall transient for 1.8% chord tip clearance..... 40
3.4 Stagnation-to-static pressure rise and blockage components and rate of change of tip blockage with repect to flow coefficient for 1.8% chord tip clearance..... 41
3.5 Passage exit plane streamwise velocity contours at points (4) and (8) for 1.8% chord tip clearance..... 42
3.6 Reversal ("backflow") of tip clearance fluid below the blade tip..... 43
3.7 Spanwise distribution of pitch averaged mass flow at passage exit plane..... 44
3.8 Leading edge tip clearance flow spillage below the blade tip..... 45
3.9 Mass flow through blade tip and spilled ahead of leading edge..... 45
3.10 Role of tip clearance backflow below the blade tip on equilibrium flow limit... 46
3.11 Contribution of tip clearance backflow to tip blockage..... 47
3.12 Indirect contribution of tip clearance backflow to tip blockage..... 48
3.13 Relative stagnation pressure deficiency of double-leaked and leading-edge spilled tip clearance fluid for point (6) in figure 3.9..... 49
3.14 Role of leading edge spillage below the blade tip on upstream propagation of backflow..... 49
3.15 Evaluation of passage equilibrium flow limit criteria for 3.0% chord tip clearance..... 51
3.16 Evaluation of passage equilibrium flow limit criteria for 1.2% chord tip clearance..... 52

4.1 Stall transient for multiple 96) blade passage configuration 58
4.2 Relative flow vectors at blade tip at time (4)..... 59
4.3 Tip clearance flow behavior in each blade passage at time (4)..... 59
4.4 Simultaneous flow events in spike formation and length-scale of spike disturbance..... 60
4.5 Axial velocity deviation at different axial location at time (4) in figure 4.1..... 62

4.6 First stage stagnation-to-static pressure rise for four-stage compressor showing stall inception type and corresponding first rotor incidence..... 63
4.7 Computed stagnation-to-static pressure rise characteristic across E3 rotor B at different tip clearances..... 63
4.8 E3 rotor B tip incidence versus flow coefficient..... 64
4.9 Effect of large tip clearance on rotor pressure rise..... 66
4.10 Effect of large rotor tip blockage on stator and stall inception type..... 66
4.11 Effect of pitch increase on E3 rotor B at 1.8% chord tip clearance..... 68

A.1 Tip clearance flow stability argument based on vortex kinematics..... 79

B.1 BTOB3D mesh of E3 rotor B blade passage geometry..... 83
B.2 BTOB3D mesh of blade tip (axial cut)..... 83

C.1 UNSTREST mesh of E3 rotor B blade passage geometry..... 89
C.2 UNSTREST mesh of blade tip (axial cut)..... 89
C.3 Single and multiple blade passage meshes..... 90

D.1 PSD analysis for 3.0% chord tip clearance at different flow coefficients..... 94
D.2 Effect of domain length on oscillation frequencies..... 95

Tables

2.1 Design parameters of the GE Low-Speed Compressor [10]..... 28
4.1 Comparison of measured [10, 25] and computed spike disturbance..... 59

Chapter 1

Introduction

1.1 Background

Compressor instabilities are a fundamental limit on gas turbine engine performance. As the mass flow through the compressor is reduced at constant speed, the pressure rise increases up to the point where instabilities (surge or rotating stall) occur as shown in figure 1.1.

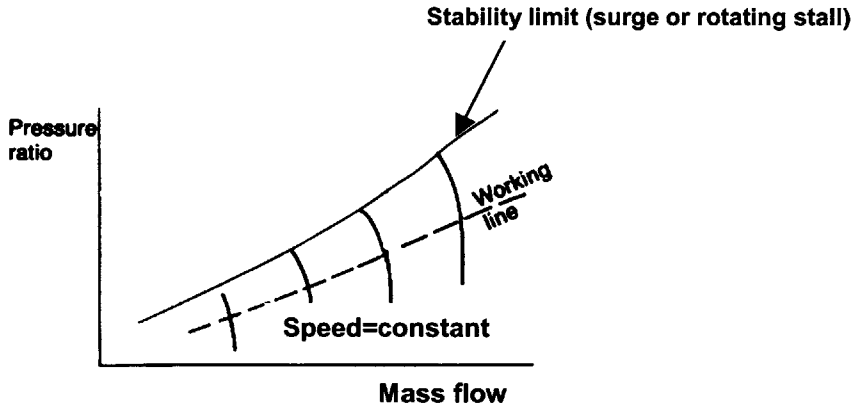

Figure 1.1. Compressor stability limit

Surge is an essentially one-dimensional axisymmetric flow oscillation accompanied by a large fluctuation in engine pressure rise. In addition to its effect on compressor performance, surge can cause damage to the engine through vibrations or excessive temperatures.

Rotating stall is a compressor instability characterized by the formation of a cell of velocity deficiency that rotates at speeds from 15-50% of the compressor rotor speed (figure 1.2). Its occurrence is usually accompanied by a drop in compressor pressure rise and engine performance as shown in figure 1.3. Recovery from stall can be different due to the presence of hysteresis.

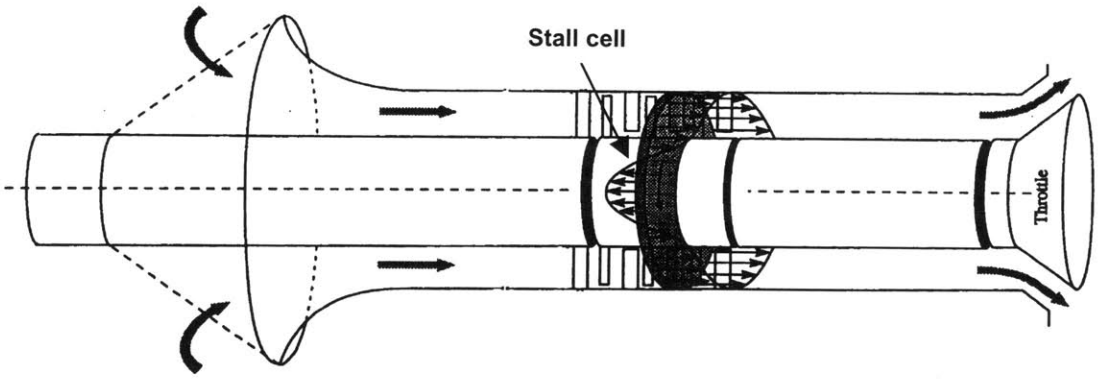

Figure 1.2. Rotating Stall

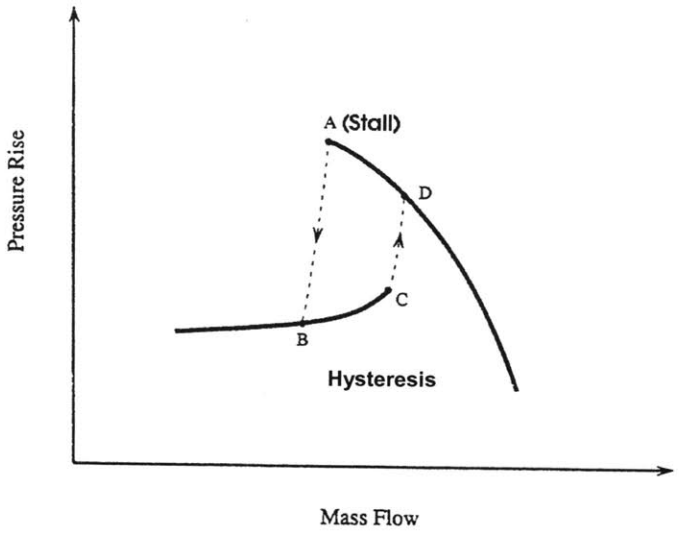

Figure 1.3. Effects of rotating stall on compressor performance

Two routes to rotating stall have been identified: long length-scale or "modal" inception and short length-scale or "spike" inception. Long length-scale stall inception is

characterized by a disturbance with a wavelength on the order of the annulus circumference, which grows into a fully developed stall cell with approximately the same rotating speed within 10 to 40 rotor revolutions. Figure 1.4 shows a measured velocity trace of modal stall inception. This type of stall inception has been successfully modeled by Moore and Greitzer [23] by considering the compression system as a combination of a duct with fluid inertia (compressor), a semi-actuator disk model of the compressor, and inviscid upstream and downstream ducts. Modal stall inception has been shown both analytically [23] and experimentally ([2], [14], [24]) to occur when the stagnation-to-static pressure rise of the compressor reaches zero-slope.

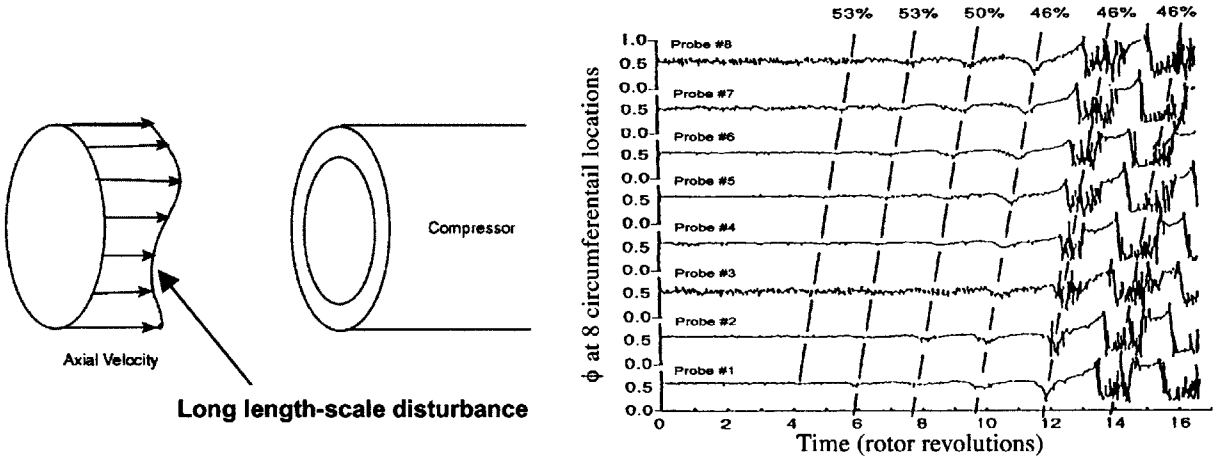

Figure 1.4. Modal stall inception and associated hot-wire (axial velocity) trace [4]

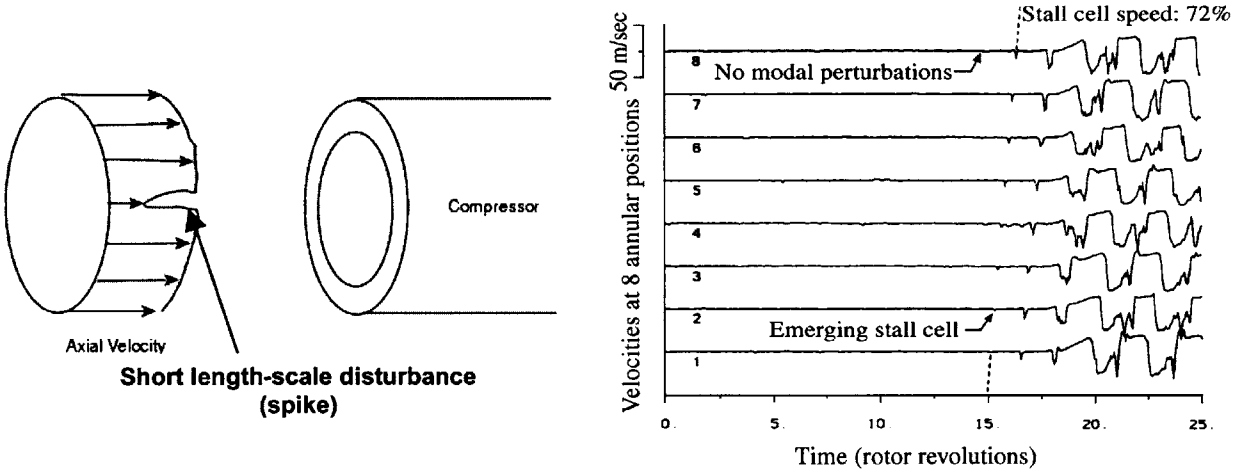

Figure 1.5. Spike stall inception and associated hot-wire (axial velocity) trace [4]

Many compressors, however, exhibit short length-scale, or spike, stall inception, which is much less understood. Figure 1.5 shows that this phenomenon, first described by Day [4], is characterized by the appearance of a disturbance (or "spike") about two to three blade pitch in width concentrated at the rotor tip. The spike rotates at about 70% of the rotor speed and grows into a two-dimensional stall cell within two to three rotor revolutions. Spike stall inception has been observed to occur before the peak of the stagnation-to-static pressure rise characteristic, i.e. in the negatively slope region of the characteristic.

Unlike long length-scale stall inception, where the small amplitude of the modal disturbance lends itself to linear analysis, the velocity defect associated with the spike disturbance is on the order of the mean velocity through the compressor and a nonlinear approach is thus required. To simulate features of the spike stall inception process, Gong *et al.* [11] modeled the compressor blades with a three-dimensional distribution of body forces generated from axisymmetric blade row pressure rise characteristics. Their results appeared to capture the growth of an *input* spike of sufficient amplitude into fully developed rotating stall. However, the origin of the spike was not resolved.

In other work, Day [4] and Camp *et al.* [2] have shown experimentally that increasing tip clearance size or reducing rotor tip incidence, both of which affects the magnitude of the tip clearance flow, can cause the compressor to change from spike to modal stall inception. Furukawa ([9], [10]) reported tip vortex breakdown near stall in computations although they did not provide a rigorous link to spike formation.

The local nature of the spike in the circumferential direction and in the tip region of the rotor leads to the idea that its origin involves the tip clearance flow, i.e. the flow that occurs from the pressure side to the suction side of a rotor blade, through the physical clearance between the blade tip and the casing. This has been shown by Storer *et al.* [29] to be a mainly pressure driven flow that emerges at the suction side with a velocity component normal to the streamwise direction (direction of the passage core flow) and rolls up into a tip vortex [3].

Stagnation pressure loss is generated by the clearance flow's interaction with the core flow below the blade tip as it exits the clearance gap. As the resulting low (relative) stagnation pressure fluid moves downstream against the blade passage pressure gradient,

blockage is generated [17], i.e. an effective reduction in the exit area of the blade passage due to the presence of low streamwise velocity fluid. Increases in blockage cause a decreases in pressure rise across the blade passage.

1.2 Problem Definition and Research Questions

The basic issue addressed in this work is the causal link between tip clearance flow and spike stall inception. Specifically, does such a link exist? If so, what is the mechanism for tip clearance flow to lead to the formation of short length-scale rotating stall disturbances? Under what conditions does this occur? The diagram in figure 1.6 depicts the problem in the context of the understanding of rotating stall.

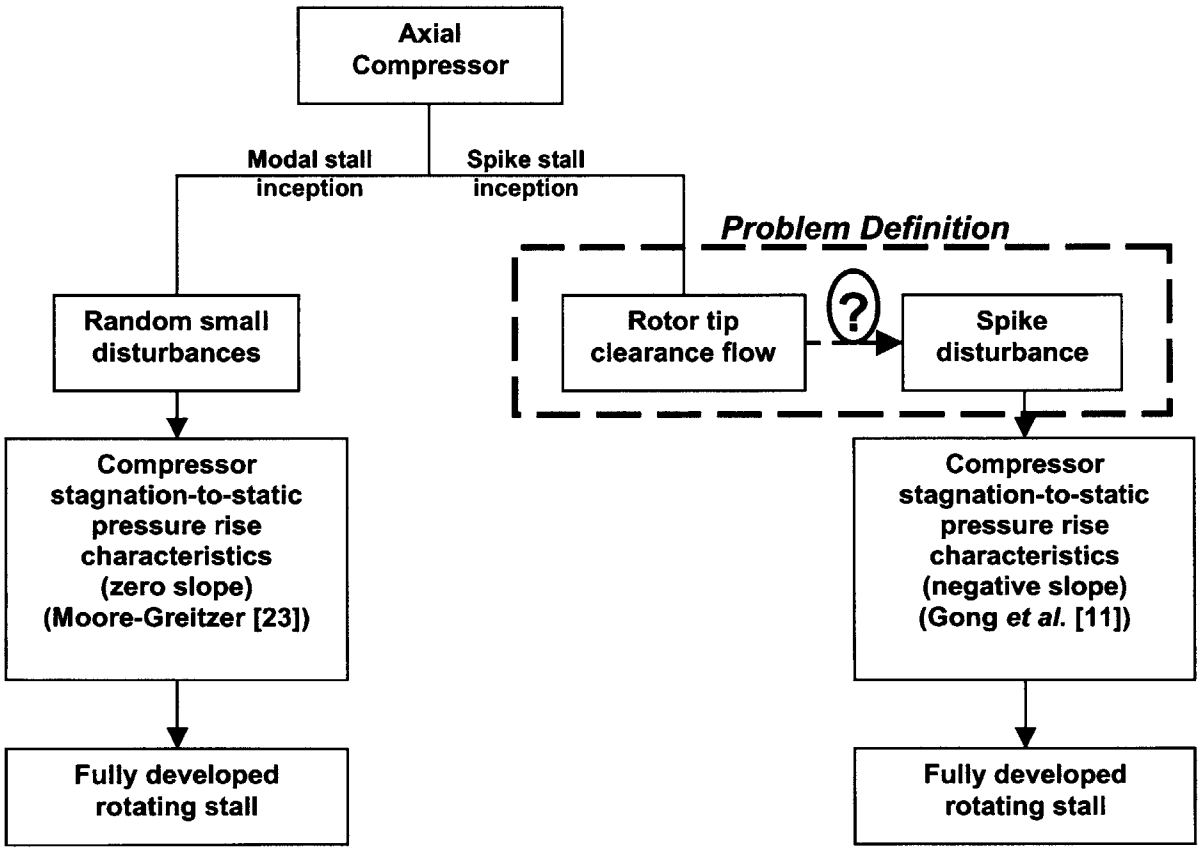

Figure 1.6. Problem definition in context of rotating stall

Figure 1.7 raises another issue, that of the usefulness of single blade passage computations in stall prediction. Single blade passage computations yield the stagnation-to-static pressure rise characteristic of the compressor and can thus be used to infer the occurrence of modal stall inception at the zero-slope peak of the stagnation-to-pressure rise characteristics. Gong's computational model [11] can predict the spike's evolution to a full stall cell given *input* pressure rise characteristics for each blade row and an *input* spike disturbance. Last but not least, tip clearance flow is a blade passage flow feature that can be captured by single blade passage computations. The issue is thus to define the conditions under which single blade passage computations can be used to predict the formation of spike disturbances, and rotating stall in general. If these conditions are established, then single blade passage computations may not only form an inexpensive predictive tool for both types of stall inception but also permit the designer to explore ways to prevent or delay rotating stall.

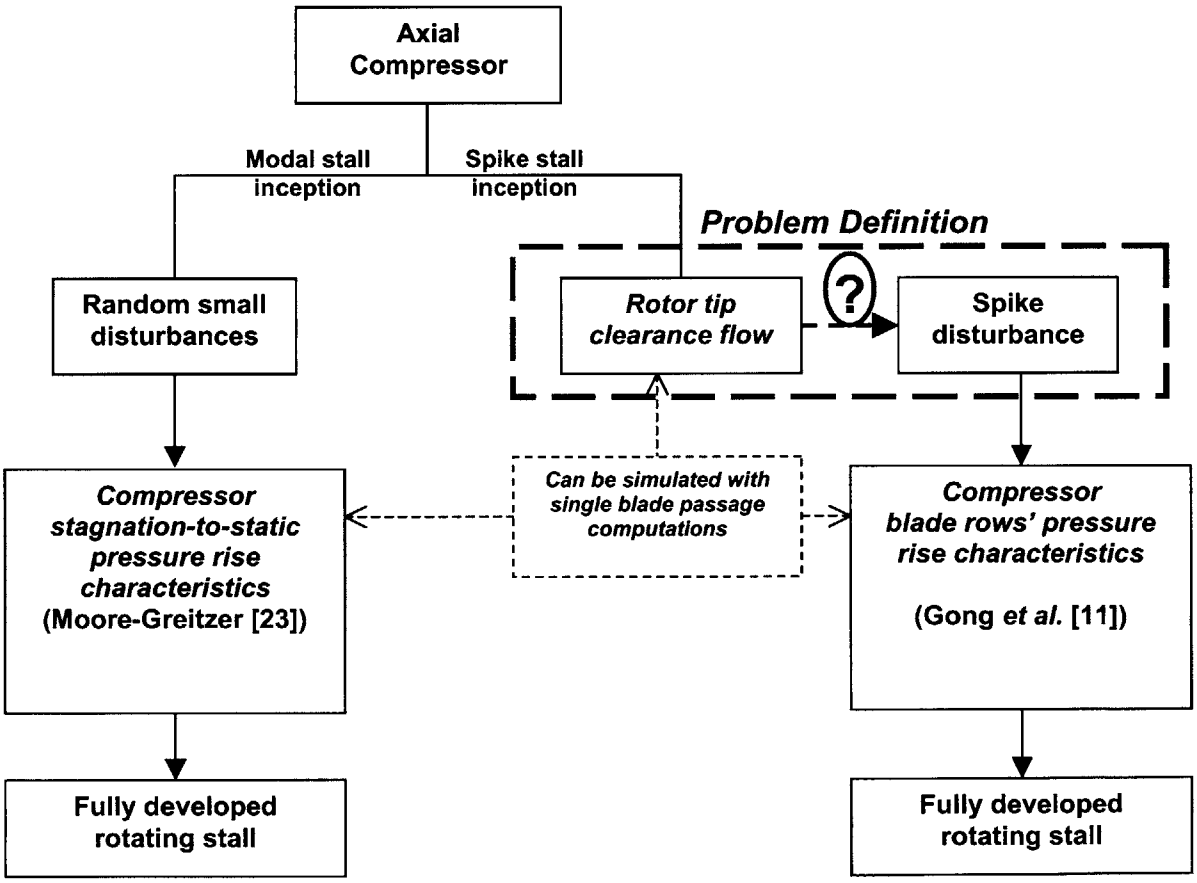

Figure 1.7. Potential of single blade passage computation in stall prediction

1.3 Research Objectives

The following are the research objectives:

Primary objective: Define the role of tip clearance flow on axial compressor instability, particularly with respect to the formation of short length-scale rotating stall disturbances

Secondary objective: Assess the role of single blade passage computations in axial compressor stall prediction

1.4 Approach

To examine the evolution of the flow field within the entire rotor blade passage around the stall point, a mainly computational approach has been taken. As discussed earlier, the local nature of short length-scale disturbances points to their possible origin in the rotor blade passage flow structures associated with the tip clearance flow. As such, computations on a single rotor blade passage configuration were used as a starting point for the study. Three reasons can be given in support of this strategy:

(1) The spike's origin is in the rotor and for the initial assessment the flow distortions introduced by adjacent blade rows do not appear to be central.

(2) The tip clearance flow structure can be captured with single passage computations.

(3) Comparing the behavior of the tip clearance flow during the transient beyond the single blade passage equilibrium solution limit* and during the stall

* Henceforth, the "equilibrium solution limit" or "equilibrium flow limit" is defined as the point of lowest mass flow for which an equilibrium state solution with constant time-mean mass flow exists. For time-accurate computations, this definition includes operating points with periodic oscillations in mass flow about a mean value.

inception transient in a multiple passage computation will provide the means to examine the link between the single passage equilibrium flow limit and spike formation.

The general methodology is as follows. First, the single passage equilibrium solution limit is obtained with time-accurate computations. Using this solution as an initial condition, the mass flow is reduced and the evolution of the transient flow field is analyzed. To simulate spike stall inception, multiple blade passage computations are performed (on the same rotor configuration) with the single blade passage equilibrium solution limit as the initial condition. The flow field in the passage where the spike disturbance occurs is compared with single blade passage results to establish the link between tip clearance flow, single blade passage computation equilibrium solution limit and spike disturbances.

The basic computational features judged necessary for this study are:

(1) Boundary layer separation: ability to capture blade boundary layer separation and corner separation, which are also potential causes of stall, so as not to prejudice the results in favor of tip clearance flow.

(2) Inlet boundary conditions: uniform inlet stagnation pressure and temperature and axisymmetric spanwise swirl distribution are used. Inlet flow distortion does not appear to be central to this initial assessment of spike stall inception.

(3) Exit boundary condition: the exit static pressure at the shroud, plus radial equilibrium is adequate given that spike disturbances usually occur while the exit static pressure is still increasing (negative slope of stagnation-to-static pressure rise characteristic) [2].

(4) Time accuracy: time accuracy is required to capture the transient flow field beyond the single passage equilibrium limit and stall inception in a multiple blade passage computation.

1.5 Thesis Organization

The first step in this study, detailed in chapter 2, is to determine the important generic flow features postulated to be linked to spike disturbances. The goals are (1) to enable the design of computations that capture these features, and (2) to focus these computations and analysis on one compressor rotor geometry. Single blade passage steady computations are obtained for rotor configurations associated with spike and modal stall inceptions. The passage flow features at the equilibrium flow limit that are common to all configurations linked with spike stall inception are identified.

The second step, covered in chapter 3, consists of time-accurate single blade passage computations that are performed up to and beyond the equilibrium solution limit, to enable the assessment of the behavior of the tip clearance flow past the equilibrium solution limit. A flow mechanism and quantitative criteria that set the single passage equilibrium flow limit are identified.

Chapter 4 clarifies the link between tip clearance flow, single blade passage equilibrium flow limit, and spike disturbances. Multiple blade passage computations are performed starting from the single passage equilibrium solution limit to show that the mechanism and criteria setting this limit leads to the formation of spike disturbances. The proposed mechanism for spike formation is then assessed for consistency with published experimental observations on stall inception.

The link between tip clearance flow and spike disturbances and its implications are summarized in chapter 5. Recommendations on how to make the identified mechanism and criteria for spike formation more applicable for generic multi-stage compressors are proposed.

1.6 Contributions

The novel aspect of this work is the use of computational fluid dynamics to extract previously unknown flow features associated with the formation of spike disturbances that could not easily be identified with experiments.

The primary contributions of the present thesis are:

(1) A mechanism linking tip clearance flow to the single blade passage equilibrium flow limit and the occurrence of spike disturbances which is consistent with experimental observations on stall inception is identified

(2) Criteria setting the single blade passage equilibrium solution limit and marking the onset of spike rotating stall disturbances are established to define the conditions for spike stall inception

The secondary contributions are:

(3) The role of single blade passage computations in stall prediction is defined

(4) Some implications of the proposed mechanism for spike formation on techniques for axial compressor operating range extension are presented

Chapter 2

Generic Passage Flow Features Associated with Spike Stall Inception

In this chapter, we identify the generic features associated with spike stall inception. Doing this serves two purposes: (1) to enable the design of computations that accurately capture these features to look into the onset of spike rotating stall disturbances, (2) to focus computations and analysis on one compressor rotor geometry, to make the endeavor of uncovering the link between tip clearance flow and spike formation practical in terms of time without foregoing the generic nature of the study.

2.1 Pertinent Flow Characteristics

The aspects of the passage flow field that are deemed to be pertinent to spike stall inception based on current knowledge are:

(1) Slope of Stagnation-to-Static Pressure Rise Characteristic: Experimental investigations into stall inception by Camp *et al.* [2] point to the fact that spike stall inception occurs while the slope of the stagnation-to-static pressure rise characteristic of the compressor is negative. For single rotor blade passage computations, the computed stagnation-to-static pressure rise characteristic of the rotor is available, but not that of the entire compressor. However, if the stagnation-to-static pressure characteristic slope of the rotor is negative at the equilibrium solution limit, i.e. the exit pressure is still increasing, one can infer spike stall inception. This is because the exit static pressure boundary

condition used in the computations is not a factor in reaching the equilibrium solution limit. In other words, the exit pressure condition allows the pressure rise of the passage to be further increased but the blade passage flow field has reached its physical pressure rise capability.

(2) Blade boundary layer near blade tip: From their observation that spike stall inception always occurred at a particular value of blade tip incidence, Camp *et al.* [2] conjectured that localized flow separation is at the source of spike stall inception. If so, blade boundary layer separation at the tip may lead to spike rotating stall disturbances. Thus, the suction surface flow field should be examined for the occurrence of or imminent boundary layer separation. The span position chosen should be close to the blade tip but far enough to not influenced by the entrainment effect of the tip clearance flow on the blade boundary layer fluid as shown in figure 2.1. Computations show that one tip clearance size below the blade tip is sufficient.

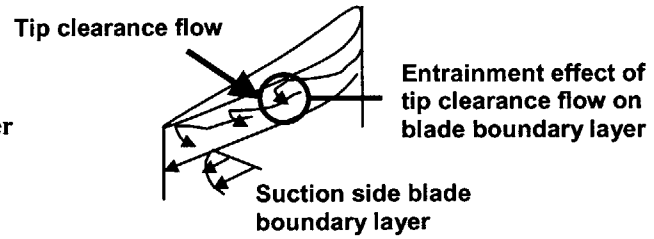

Figure 2.1. Blade boundary layer below blade tip

(3) Interface between incoming and tip clearance flow: The role of the tip clearance flow on the formation of spike stall inception is at the heart of this investigation. The following is a brief discussion of tip clearance flow that defines the main feature(s) to examine in relation to spike stall inception. As described in chapter 1, tip clearance flow is the pressure driven flow through the clearance between the rotor and the casing. Figure 2.2 is a sketch of the path followed by a fluid particle as it comes from upstream near the pressure side. It emerges on the suction side (along with other fluid particles all along the blade chord) with a velocity component normal to the streamwise (passage core flow) direction. Interaction (shear/mixing) with the streamwise core flow below the clearance leads to a stagnation pressure loss and entropy rise in the

tip clearance fluid. The tip clearance fluid rolls up into a tip vortex with a low streamwise velocity component in the vortex, which creates tip clearance blockage.

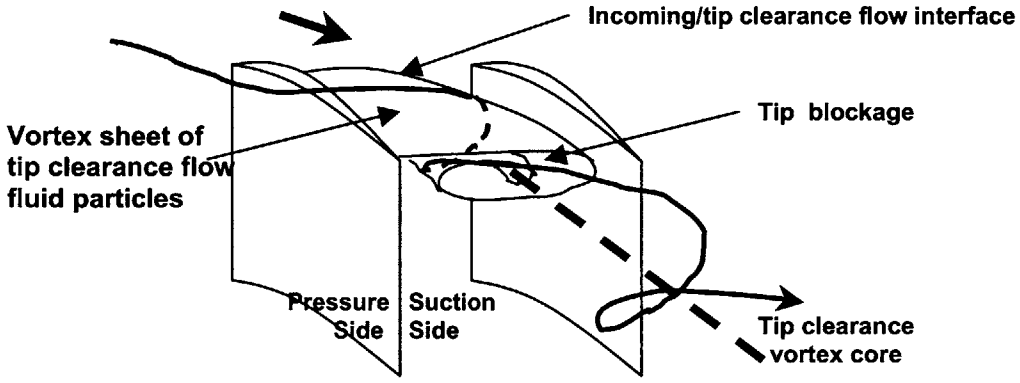

Figure 2.2 Basic features of tip clearance flow

The three basic flow features of the tip clearance flow, namely blockage, tip vortex and interface with the incoming flow, are identified in figure 2.2. The tip clearance blockage is reflected in the shape of the stagnation-to-static pressure rise characteristic. The hypothesis that linked tip vortex kinematics to spike formation [15] does not appear to be relevant for compressor rotors as discussed in appendix A and it is the interface between the incoming and tip clearance flows is of interest. This surface separates the low-entropy incoming flow from the high-entropy tip clearance flow. It can be traced as a region of high entropy gradient using entropy contours (figure 2.3).

Khalid *et al.* [17] showed that the trajectory of this interface can be estimated from the balance between the momentum of the incoming and tip clearance flows. As the incoming mass flow is reduced, the axial momentum of the incoming flow is reduced, while the axial momentum of the tip clearance flow increases from increased blade loading. The result is the movement of the interface towards the rotor leading edge plane, observed experimentally by Koch [18]. Analysis by this author of the multiple blade passage stall simulation data by Hoying *et al.* [15] shows that this incoming/tip clearance flow lines up with the rotor leading edge plane near the

blade tip radius at the stall point. The entropy contour at the blade tip radius will thus be plotted at the equilibrium flow limit for each rotor configuration.

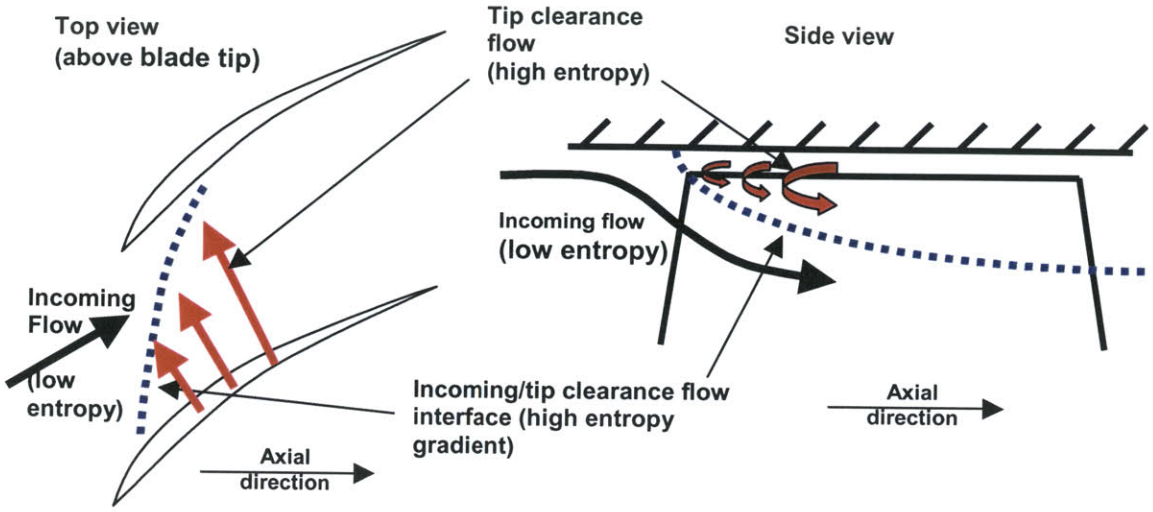

Figure 2.3. Interface between the incoming flow and the tip clearance flow

2.2 Low-Speed Compressor Rotor

The geometry examined is the GE E3 rotor B, which forms the first rotor for a low-speed compressor tested at the General Electric Aerodynamic Research Laboratory [31]. The compressor has constant hub and tip radii and consists of four repeating stages preceded by inlet guide vanes (IGV) to impart swirl to the first rotor. The compressor's design parameters are given in table 2.1. This compressor has been experimentally shown to exhibit short length scale stall inception with spikes originating in the first rotor [27]. The tip Mach number is approximately 0.2 and the Reynolds number based on blade chord is 300,000.

Table 2.1 Design parameters of the GE Low-Speed Compressor [11]

Parameter	IGV	Rotor	Stator
Number of blades	110	54	74
Stagger angle (deg)	10	50	40
Solidity (mid-span)	1.4	1.16	1.43
Hub-to-tip ratio	0.85	0.85	0.85

To look at the effect of tip clearance flow on this compressor rotor stall behavior, the simplest method is to vary the rotor tip clearance size. Steady-state computations were carried out for the E3 rotor B geometry at different tip clearances to identify cases associated with spike and modal stall inception based on the slope of the stagnation-to-static pressure rise characteristics at the equilibrium solution limit. A negative slope was associated with spike stall inception, and a zero or positive slope with modal stall inception. In this process, the stagnation-to-static pressure rise characteristics needed to be computed along a speedline for many tip clearance sizes. A steady-state code and a computationally coarse grid are used to minimize run time requirements. The steady code was BTOB3D, written by Professor W.N. Dawes of Cambridge University. It is a widely used code designed to give good solutions with coarse meshes. To further increase computational speed, the blade tip Mach number was increased to 0.5. This brings the Reynolds number to 850,000 but does not alter the physics behind the problem*. The boundary conditions are as described in chapter 1. At the inlet, the radial axisymmetric swirl distribution is given by the spanwise exit angle distribution taken from the inlet guide vanes (IGV), and uniform inlet stagnation temperature and pressure are used. Details of the code, mesh and computational procedure are presented in appendix B.

2.2.1 Spike Stall Inception

Steady-state single blade passage computations for E3 rotor B at tip clearance sizes varying from 0.9 to 3.0% chord have identified a range of clearances between 1.2-1.35% chord where the slope of the stagnation-to-static pressure rise coefficient is clearly negative at the equilibrium solution limit. The pertinent flow characteristics described in section 2.1 can be examined for the sample case of 1.2% chord tip clearance. Figure 2.4a is the stagnation-to-static pressure rise characteristic, showing negative slope at the equilibrium solution limit. Throughout this study, the stagnation-to-static pressure rise coefficient is defined as the difference in area-averaged rotor exit static pressure and mass-averaged rotor inlet stagnation pressure, non-dimensionalized by the dynamic

* The effect of Reynolds number on the tip clearance flow structure and its influence on the stalling point is minimal at large Reynolds numbers. Koch [18] showed that for the Reynolds numbers in the range of 1.3×10^5 to 10^6, the change in maximum pressure rise coefficient is only 4%.

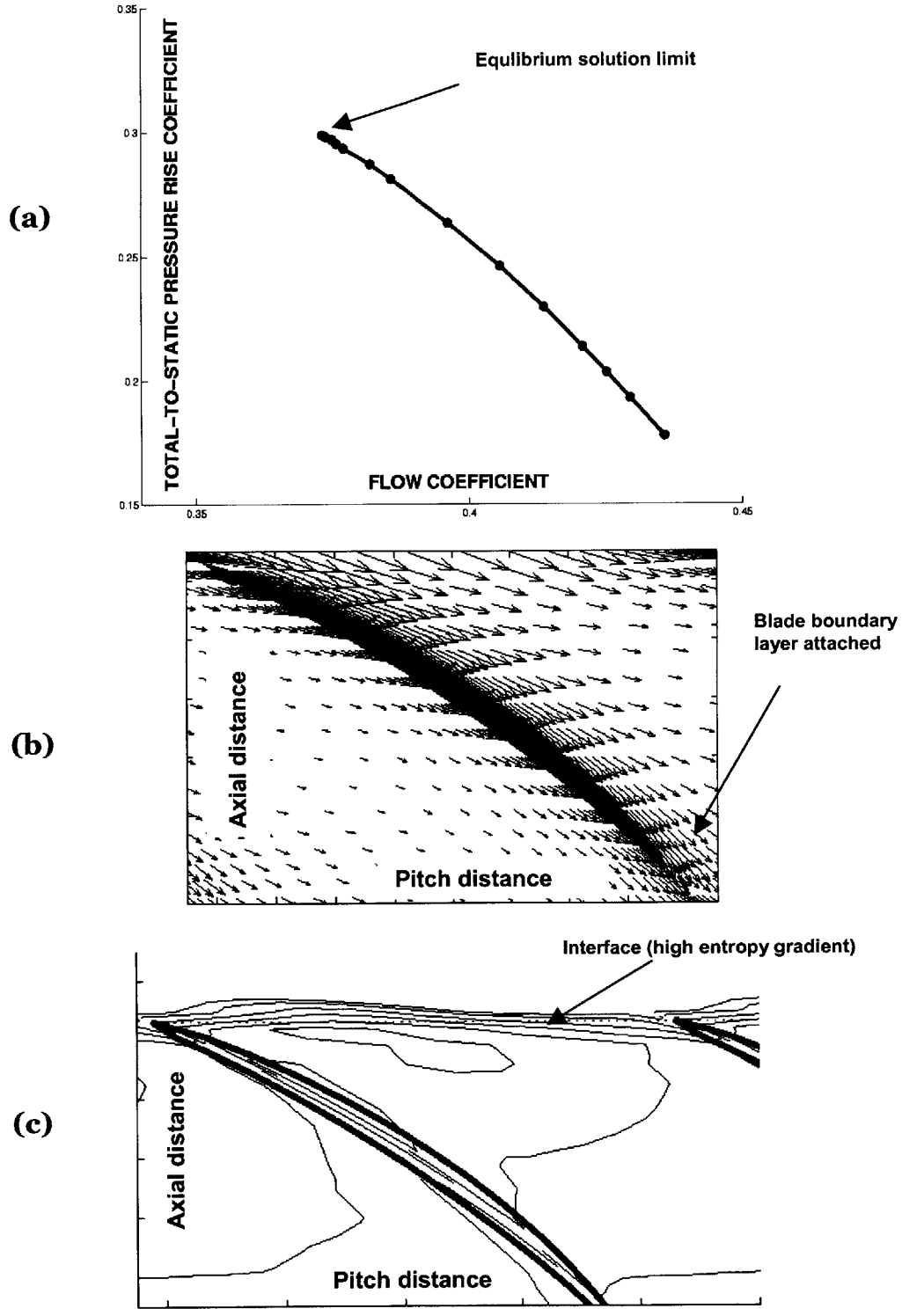

Figure 2.4. **E3 rotor B steady single blade passage computations at 1.2% chord tip clearance. (a) Stagnation-to-static pressure rise characteristic. (b) Flow field relative to rotor at one tip clearance distance below blade tip at equilibrium solution limit. (c) Entropy contour at blade tip radial plane at equilibrium solution limit.**

(a)

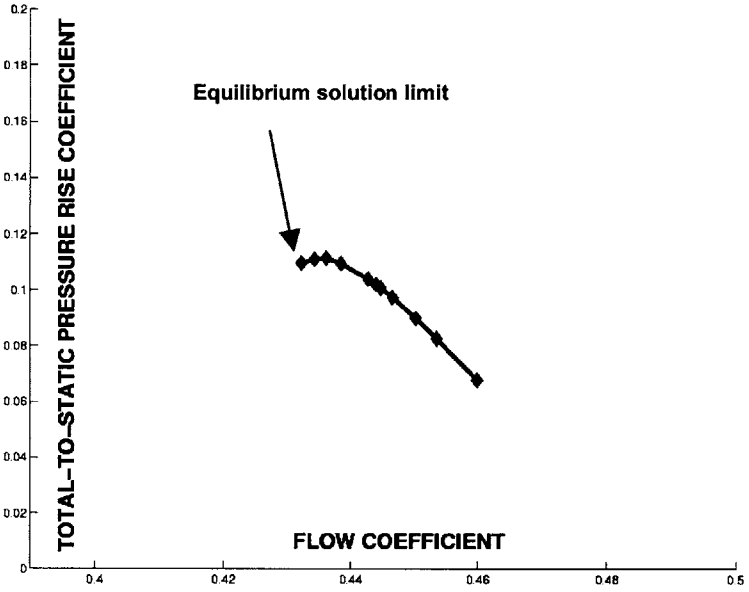

(b)

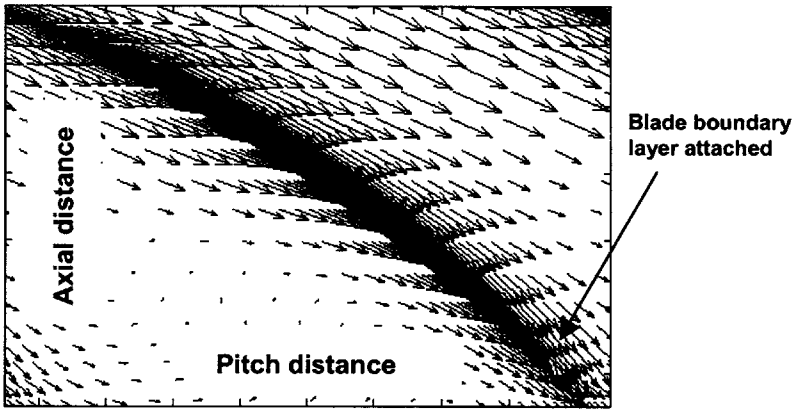

(c)

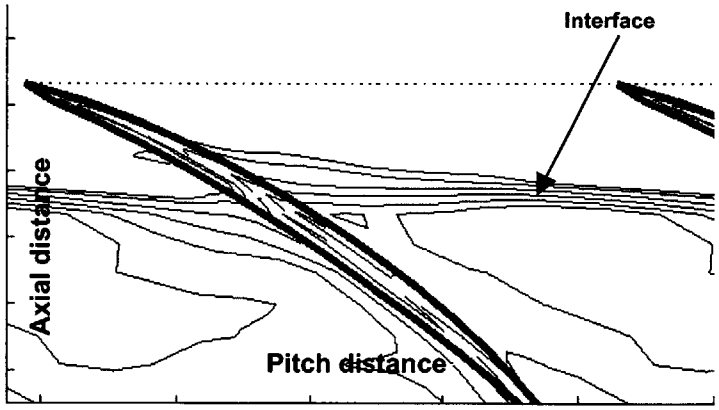

Figure 2.5. E3 rotor B steady single blade passage computations at 3.0% chord tip clearance. (a) Stagnation-to-static pressure rise characteristic. (b) Flow field relative to rotor at one tip clearance distance below blade tip at equilibrium solution limit. (c) Entropy contour at blade tip radial plane at equilibrium solution limit.

pressure based on inlet density and blade tip speed. The mass-averaged inlet stagnation pressure is used because it is the physical quantity that is conserved from the domain inlet to the rotor leading edge, in the absence of viscous losses. The area-averaged static pressure represents the force on the trailing edge rotor plane. Due to their physical nature, these averages were thus used to reduce the three-dimensional pressure rise of the passage into a one-dimensional pressure rise characteristic required to infer stall inception type. The flow coefficient is defined as the rotor inlet average axial velocity divided by rotor tip speed. Figure 2.4b presents the velocity vectors in the rotor frame of reference at one tip clearance below the blade tip. The boundary layer on the suction side is attached with no sign of separation at the trailing edge. Last but not least, figure 2.4c plots the entropy contours at the blade tip radial plane to determine the location of the incoming/tip clearance flow interface, which lines up with the rotor leading edge plane.

2.2.2 Modal Stall Inception

Figure 2.5 gives information for the E3 rotor B single blade passage computations at 3.0% chord tip clearance. There is a slightly positive slope of the characteristic at the equilibrium solution limit (figure 2.5a). Day [4] showed that stall inception type changes from spike to modal as tip clearance is increased. The positive slope at the equilibrium solution limit and large tip clearance size (compared to the case in section 2.2.1) thus associate this case with modal stall inception. The blade boundary layer is also well attached (figure 2.5b). The incoming/tip clearance flow interface is well inside of the blade passage (figure 2.5c), which contrasts with the cases associated with spike stall inception (figure 2.4c).

2.3 High-Speed Compressor Data

In this section the generic nature of the observations about the blade boundary layers and incoming/tip clearance flow interface from the E3 rotor B geometry is assessed for high-speed compressor rotor geometries. The data are steady-state single blade passage computations performed by NASA and Pratt & Whitney for Rotor 35 and

Rotor 37, respectively, using their in-house codes. Rotor 35 and Rotor 37 belong to the same family of transonic rotors. Rotor 35 has a tip Mach number of 1.3, a hub-to-tip ratio of 0.7 and a solidity of 1.47. More information can be found in reference [28].

2.3.1 Spike Stall Inception

Rotor 35 in a *single stage* configuration exhibits modal stall inception. However, Spakovszky *et al.* [28] showed that at 85% speed with inlet stagnation pressure radial distortion using a screen in the outer radius, this compressor exhibited spike stall inception with a negative slope of the stagnation-to-static pressure ratio (equivalent to stagnation-to-static pressure rise characteristic) as shown in figure 2.6a. Steady single rotor passage computations with the same inlet total pressure distortion as Spakovszky's experiment for Rotor 35, obtained from NASA, were analyzed at the equilibrium solution limit, which matches the experimental stall point to within 6% in corrected mass flow. Figure 2.6c shows that the common flow feature with the E3 rotor B (figure2.4c) is that the incoming/tip clearance flow interface lines up with the rotor leading edge, while the presence of suction side boundary layer separation in figure 2.6b, and not in figure 2.4b, shows that boundary layer separation is not a generic flow feature associated with spike stall inception.

2.3.2 Modal Stall Inception

Figure 2.7 shows the same information as figure 2.6 for the steady-state single blade passage computations of Rotor 37 without inlet radial distortion, performed by Pratt and Whitney. This is a rotor geometry that exhibits modal stall inception, which is consistent with the flatness of the computed stagnation-to-static pressure rise characteristic at the equilibrium solution limit (figure 2.7a). Figures 2.7b and 2.7c show that at this point, the blade boundary layer is attached and the incoming/tip clearance flow interface is still inside the blade passage, similar to the modal stall configuration for the E3 rotor B geometry (figure 2.5c) and in contrast to that of the Rotor 35 spike stall inception case (figure 2.6c).

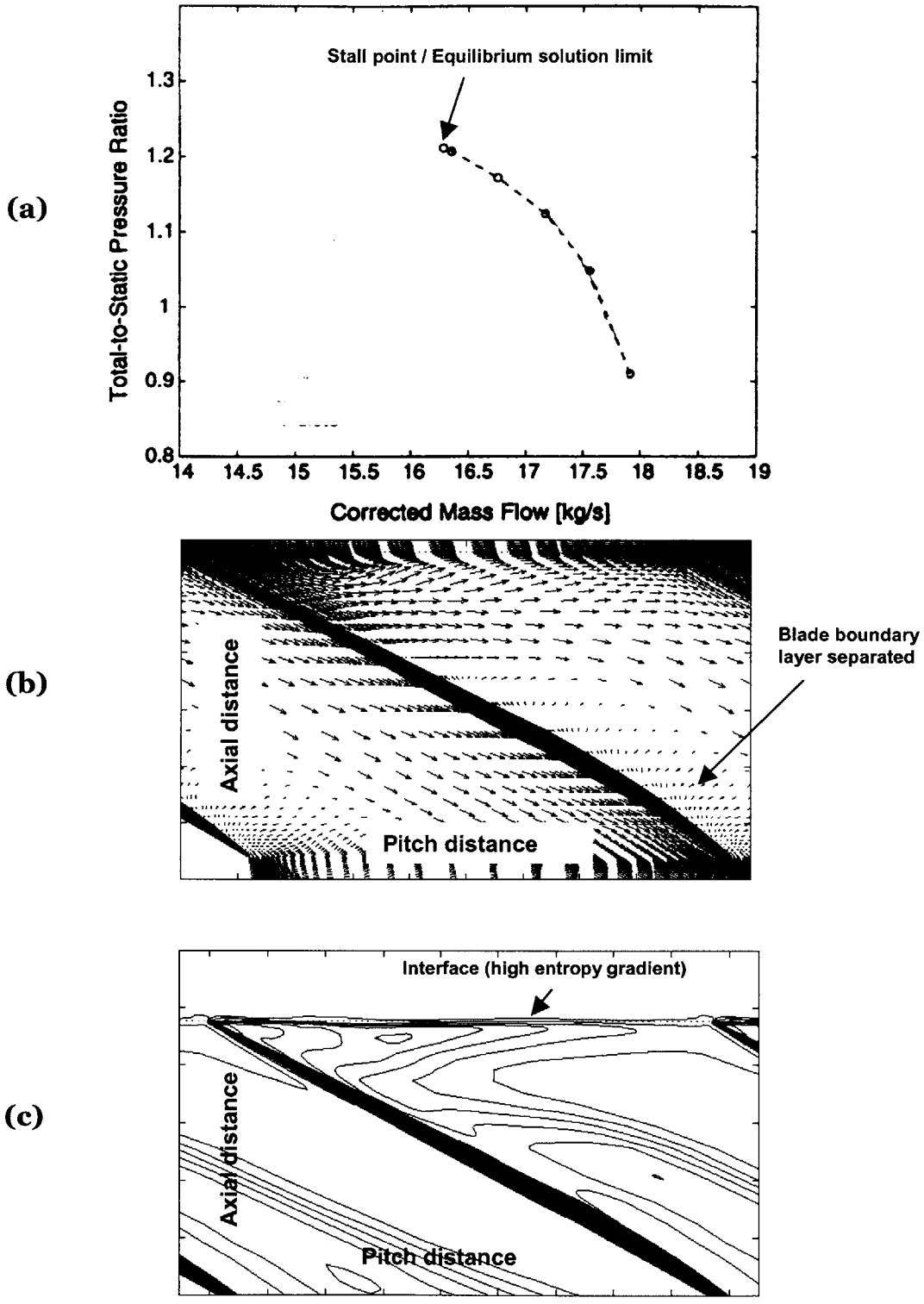

Figure 2.6. Rotor 35 steady single blade passage computations (NASA) with inlet stagnation pressure distortion. (a) Experimental stage stagnation-to-static pressure ratio (Spakovszky *et al.* [28]). (b) Flow field relative to rotor at one tip clearance distance below blade tip at last equilibrium solution. (c) Entropy contour at blade tip radial plane at last equilibrium solution.

(a)

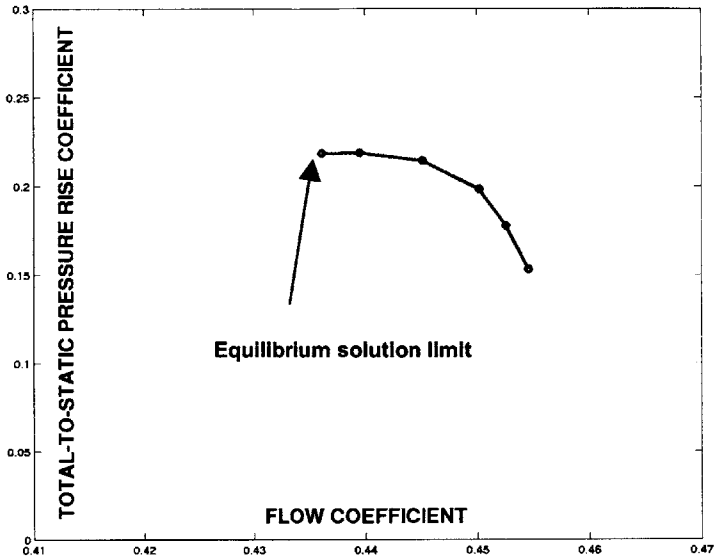

(b)

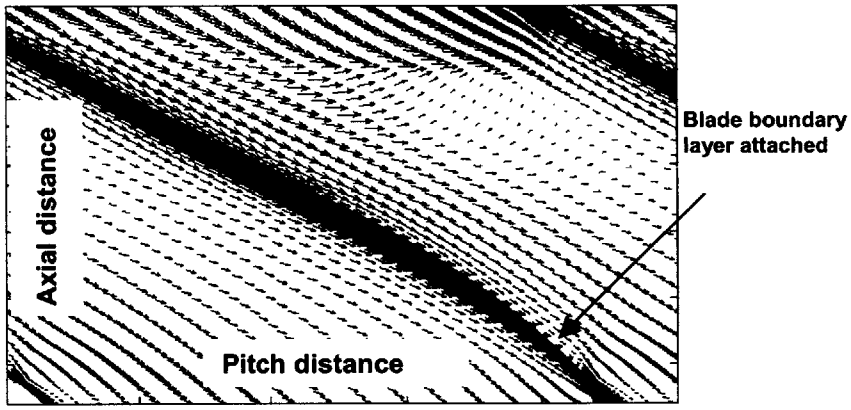

(c)

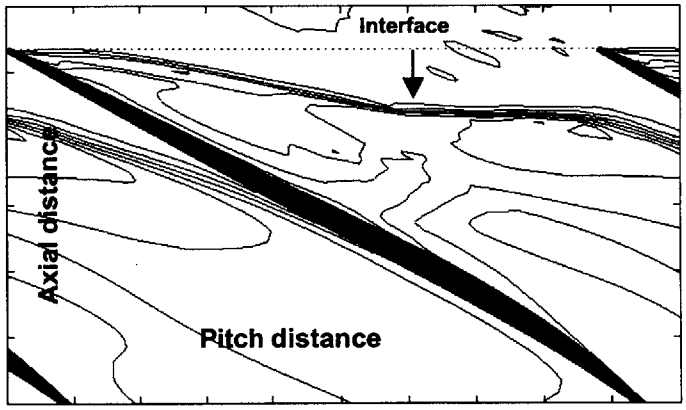

Figure 2.7. Rotor 37 steady single blade passage computations (Pratt & Whitney) without inlet stagnation pressure distortion. (a) Stagnation-to-static pressure rise characteristic. (b) Flow field relative to rotor at one tip clearance distance below blade tip at equilibrium solution limit. (c) Entropy contour at blade tip radial plane at equilibrium solution limit.

2.4 Summary

The results presented in this chapter show that a generic flow feature specific to rotors exhibiting spike stall inception is the interface between the incoming and tip clearance flow lines up with the rotor leading edge at the blade tip near stall. This is in contrast with modal stall cases where this interface lies inside the blade passage. In addition to the computational data presented, a recent piece of work on casing boundary layer by Saathoff *et al.* [26] comes to corroborate the above observation. Figure 2.8 shows the casing oil flow pattern for a low-speed single stage axial compressor near stall. This compressor has been shown to exhibit spike stall inception [8]. The incoming/tip clearance flow interface, visible as the dark line that separates the incoming and tip clearance flows, lies at the leading edge plane at the casing. Therefore, any future computations should have a fine mesh in the blade tip leading edge region to capture this incoming/tip clearance flow interface.

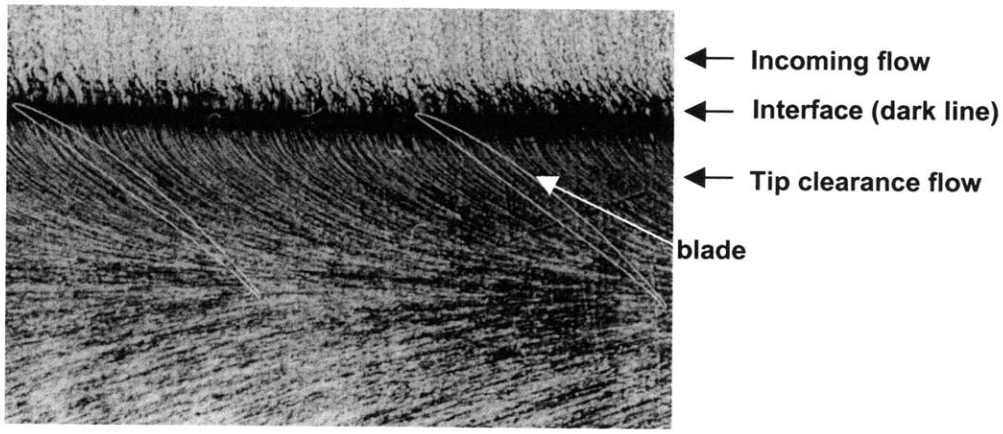

Figure 2.8. Rotor casing oil flow pattern near stall on a low-speed single-stage compressor exhibiting spike stall inception [24]

Based on the generic nature of the incoming/tip clearance interface feature, in the next chapter, single blade passage computations will be performed on the E3 rotor B configuration. Because blade boundary layer separation is not a factor (figure 2.4b), computations on this geometry will help determine the role played by tip clearance flow on the single blade passage equilibrium flow limit (chapter 3), especially in terms of the incoming/tip clearance flow interface, and on the formation of spike disturbances (chapter 4).

Chapter 3

Blade Passage Equilibrium Flow Limit

In this chapter, the mechanism that links the tip clearance flow to the single blade passage equilibrium solution limit is described. Chapter 2 showed that the generic feature associated with spike stall inception is characterized by the interface between the incoming and tip clearance flows lining up with the rotor leading edge plane at the blade tip. The E3 rotor B geometry exhibits this flow feature. This geometry also does not have blade boundary layer separation so that the role of tip clearance flow on the passage equilibrium flow limit can be isolated. Thus, a reduced set of time-accurate single blade passage computations were performed on the E3 rotor B configuration. The behavior of the tip clearance flow past the equilibrium solution limit is assessed. Threshold events marking the equilibrium solution limit are identified and a mechanism involving the tip clearance flow is provided to explain this limit. Quantitative criteria linking tip clearance flow to the single blade passage equilibrium flow limit are established.

3.1 Single Blade Passage Computations

Time-accurate computations on the E3 rotor B geometry were done using UNSTREST, written by Professor J. D. Denton of Cambridge University. A dense mesh is used within the blade passage to better capture flow features, particularly the incoming/tip clearance flow interface and any spillage of tip clearance fluid at the leading edge plane. Figure 3.1 compares the new mesh to that used the steady computations

described in section 2.2. The boundary conditions applied are as in section 2.2. Appendix C provides more information on the code, mesh and computational procedure.

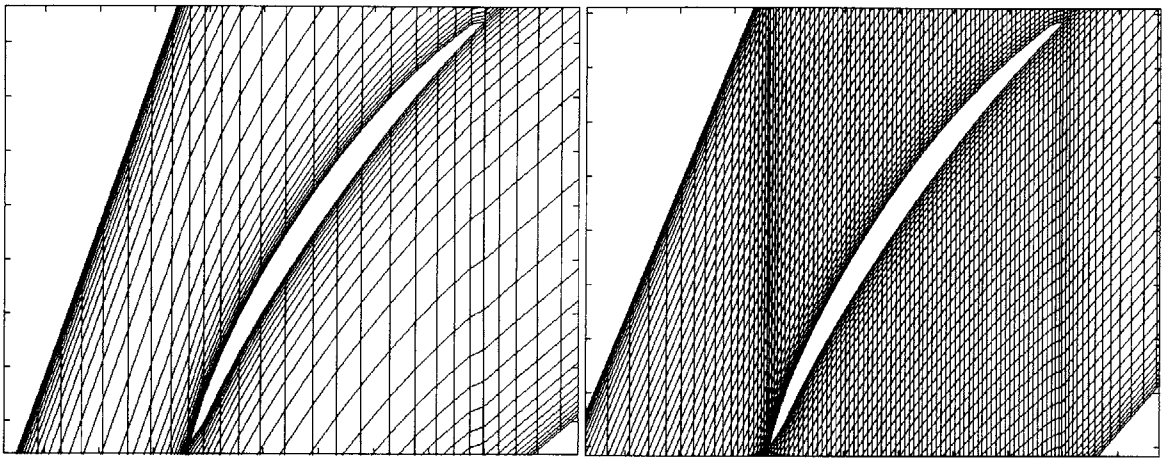

(A) Old mesh (steady computations) **(B) New mesh (unsteady computations)**

Figure 3.1. Improvement in E3 rotor B mesh for time-accurate computations

Figure 3.2 presents the stagnation-to-static pressure rise characteristic for different tip clearance sizes computed in time-accurate mode. The equilibrium solution limit is within 0.03% of the dynamic head based on blade tip speed for all clearances except 3.0% chord tip clearance. In this case, the equilibrium solution limit is computed to within 0.3% due to large oscillations in the tip clearance flow as discussed in the next paragraph.

Figure 3.2 shows that for tip clearances of 1.8% chord and above, the passage flow equilibrium limit is reached while the slope of the pressure rise is still negative*. For clearances above 1.8%, stable oscillations in the tip clearance flow (sometimes with multiple frequencies) appear. They increase in amplitude with tip clearance size and as one gets closer to the equilibrium solution limit. As discussed further in appendix D, these oscillations could have a physical origin since they are similar in nature to the tip clearance flow oscillations termed "rotating instabilities" measured experimentally by Mailach *et al.* [21] at large rotor tip clearances close to the stall point. For 3.0% chord tip

* It is noted that the feature of negative slope of the stagnation-to-static characteristic at the equilibrium solution limit starts to occur at 1.8% rather than 1.2% chord as in the steady computations in section 2.2. This discrepancy is from the difference in code as well as the difference in pinched blade tip meshes (figures B.2 and C.2) such that the corresponding effective (square) tip clearance sizes are not the same.

clearance, the oscillation amplitude reach about 2% of the dynamic head based on blade tip speed. The time-averaged speedlines are thus shown for 2.0% and 3.0% chord tip clearance sizes. The effect of the oscillations on the instantaneous pressure rise characteristic for 3.0% chord tip clearance at several operating points with one dominant frequency are also shown.

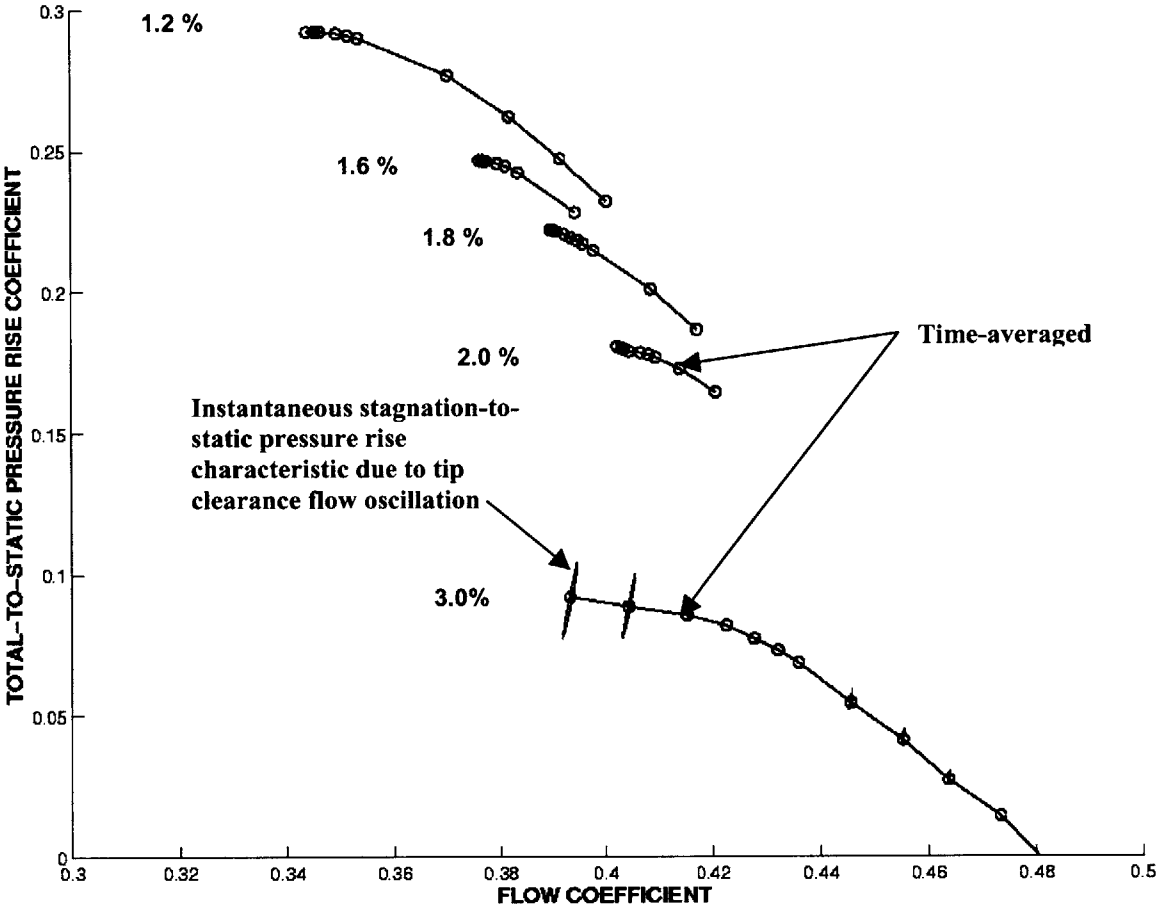

Figure 3.2. Stagnation-to-static pressure rise characteristic across E3 rotor B at different tip clearances (% chord) from single blade passage time-accurate single blade passage computations (UNSTREST)

For all cases shown in figure 3.2, equilibrium solutions exist until the interface between the incoming and tip clearance flows reaches the rotor leading edge plane. In the rest of this chapter, the equilibrium solution limit will be connected to tip clearance flow for the above cases. A quantitative assessment of the incoming/tip clearance flow interface in terms of the leading edge flow spillage will be presented. In the next chapter,

the link between the above results and stall inception, both spike and modal, will be elucidated.

3.2 Cause of Equilibrium Flow Limit

3.2.1 Tip Clearance Flow Behavior

To initiate the transient to flow coefficients below the equilibrium solution limit, the exit pressure was increased beyond the highest value for which an equilibrium solution exists. A mass flow transient occurs, as shown in figure 3.3 for the 1.8% tip clearance case. All the cases shown in figure 3.2 exhibit this behavior beyond the equilibrium flow limit.

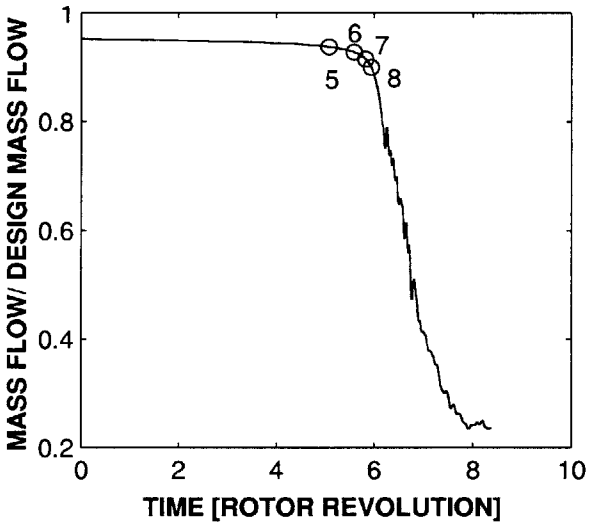

Figure 3.3. Single blade passage stall transient for 1.8% chord tip clearance

Figure 3.4a shows the stagnation-to-static pressure rise characteristic and the blockage at the blade passage exit plane for the 1.8% chord tip clearance case. Blockage is computed according to the formulation proposed by Khalid *et al.*[17], using the streamwise velocity components and gradients, analogous to displacement thickness for a boundary layer in unidirectional flow. The blockage is separated into that associated with the tip clearance flow and the blade passage boundary layer, which includes the boundary layers on the blade and hub. Operating point (4) is the equilibrium solution limit and is marked by a vertical dotted line. Points (1) through (4) represents equilibrium flow conditions, whereas points (5) through (8) are transient flow conditions as shown by their respective mass flows in figure 3.3.

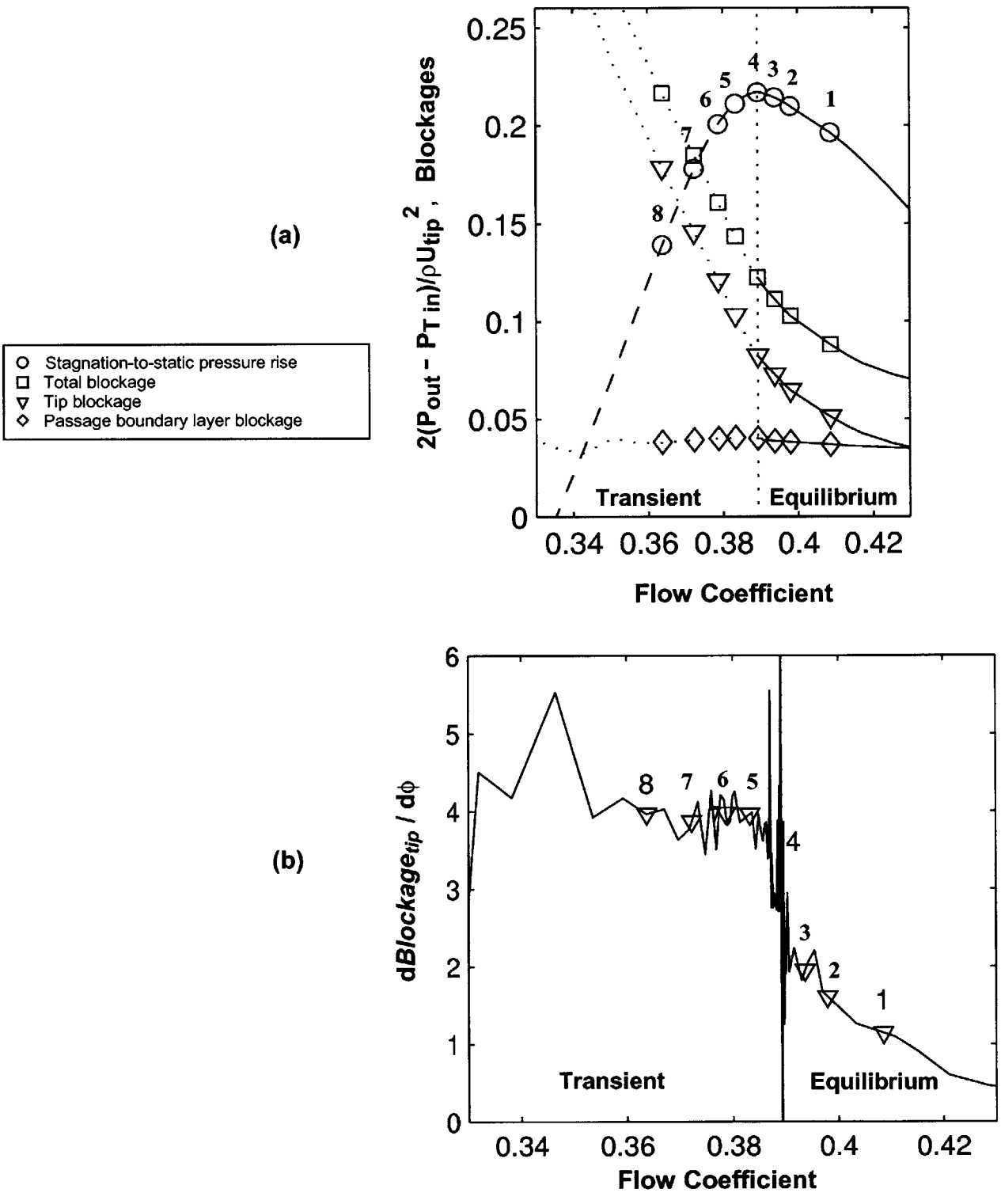

Figure 3.4. Stagnation-to-static pressure rise and blockage components (a), and rate of change of tip blockage with respect to flow coefficient (b) for 1.8% chord tip clearance

The equilibrium solution limit (point (4)) marks the onset of a rapid growth in total blockage (figure 3.4a). The growth of tip clearance blockage (tip blockage) accounts for all of the growth in total blockage, whereas the blockage from the passage boundary layer (*total blockage - tip blockage*) does not grow beyond the equilibrium solution limit. This behavior is confirmed by the streamwise velocity contours at the blade passage exit plane for operating points (4) and (8) in figure 3.5. The velocity contours show that the tip blockage region grows from the tip towards the hub, and that the blade and hub boundary layers remain unchanged. The growth in tip blockage is also shown in figure 3.4b, which exhibits a jump in the rate of tip blockage rise ($dBlockage_{tip}/d\phi$) with respect to flow coefficient at the equilibrium solution limit.

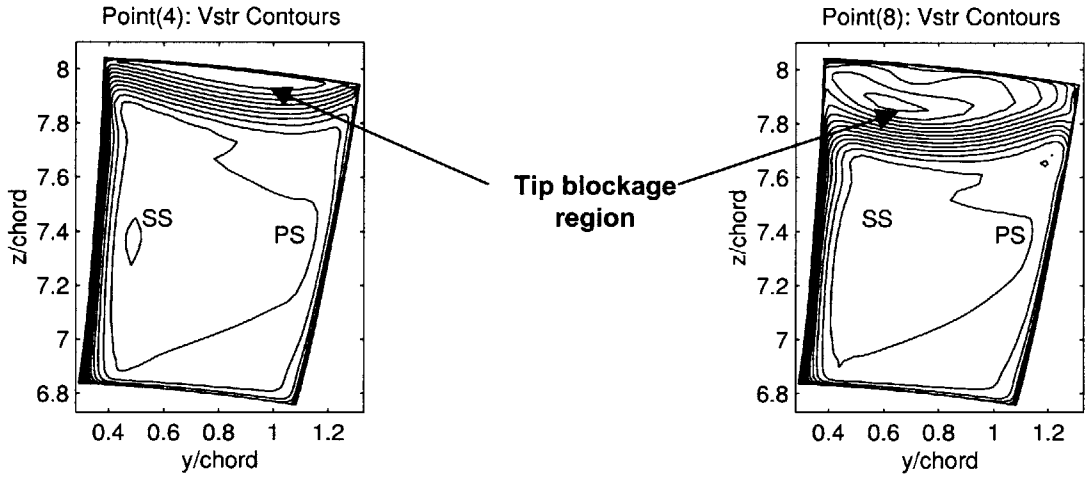

Figure 3.5. Passage exit plane streamwise velocity contours at points (4) and (8) for 1.8% chord tip clearance

The remainder of section 3.2 focuses on the mechanism that leads to the onset of the increase in tip clearance blockage beyond the equilibrium solution limit, including the source of this blockage increase. In this we focus on one particular tip clearance, 1.8% chord, because of two important aspects. First, its stagnation-to-static pressure rise characteristic has a negative slope at the last equilibrium solution (figure 3.2). Second, it does not exhibit any oscillations so the clearance flow behavior is more readily examined. We first identify the two threshold flow events that mark the equilibrium flow limit (section 3.2.2). Their contributions to the onset of the described tip clearance flow

evolution are covered in section 3.2.3 and 3.2.4. Criteria that set the last single blade passage equilibrium solution are established and shown to apply to other tip clearance sizes in section 3.2.5.

3.2.2 Threshold flow events

Two flow events occur in the flow transient beyond the equilibrium flow limit. One is tip clearance flow from adjacent blade passages flowing back into a blade passage at the trailing edge as depicted in figure 3.6. The schematic shows the path of a tip clearance flow fluid particle that travels along the outer envelope of the tip clearance flow region. After leaving the trailing edge of this blade passage, the particle flows into the next blade passage below the blade tip radius such that it impinges on the pressure surface. Henceforth, this reversal of the tip clearance fluid from adjacent blade passages is referred to as "tip clearance backflow".

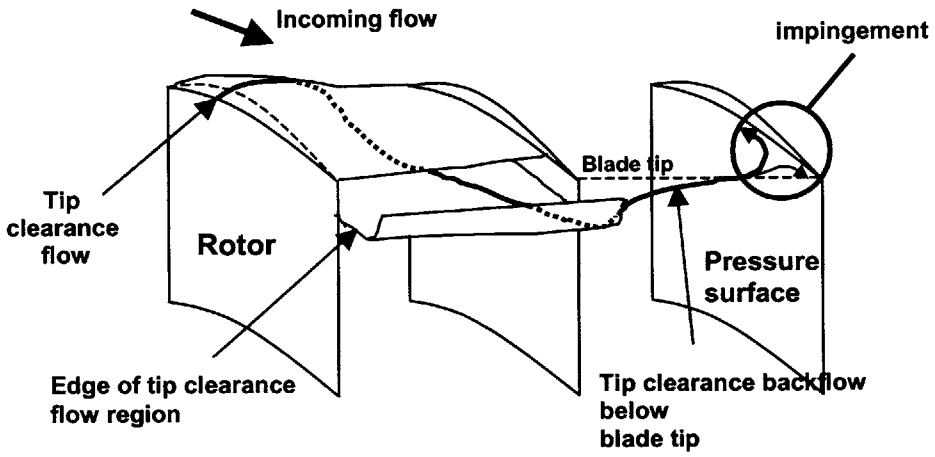

Figure 3.6. Reversal ("backflow") of tip clearance fluid below the blade tip

Figure 3.7 shows the onset of tip clearance backflow below the blade tip at the equilibrium flow limit. Figure 3.7 plots the spanwise distribution of pitch-averaged mass flow. The operating point numbers correspond to those on figures 3.3 and 3.4. The mass flow per unit pitch is non-dimensionalized by inlet stagnation flow density times blade tip

speed. For equilibrium solutions (points (1) through (3)), figure 3.4 shows downstream (positive) mass flow below the blade tip. However, at the equilibrium solution limit (point (4)), the net mass flow reaches zero at the blade tip and becomes negative for transient points at lower flow coefficients (points (5) through (8)), which indicates backflow below the blade tip.

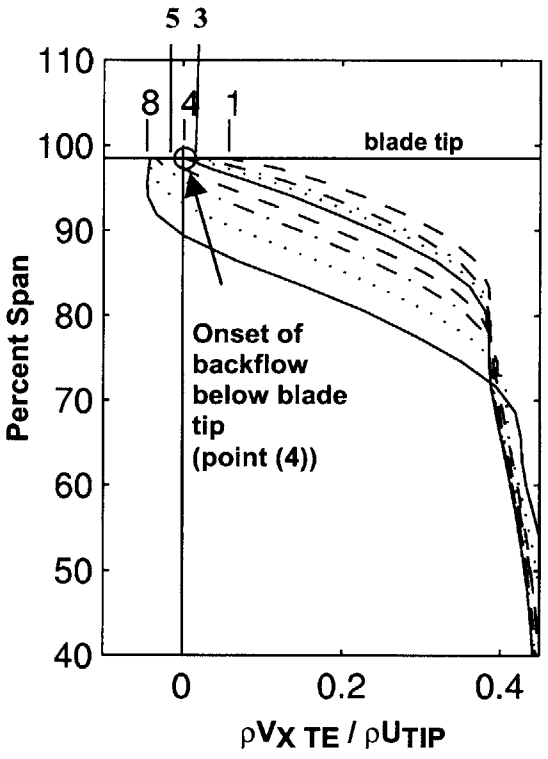

Figure 3.7. Spanwise distribution of pitch-averaged mass flow at passage exit plane (1.8% chord tip clearance)

The other threshold event is the spillage of tip clearance flow to the adjacent blade passage ahead of the rotor leading edge and below the blade tip radius. This is depicted in figure 3.8, which shows the path of a tip clearance flow fluid particle that travels along the outer envelope of the tip clearance flow region and spills into the next blade passage. Figure 3.9 plots the mass flow of the fluid flowing over the blade tip and the mass flow spilling ahead of the blade leading edge below the blade tip for the operating points shown in figure 3.4a. The curves, normalized by blade passage mass flow, show that the amount of spilled fluid increases while that of the fluid flowing over the blade tip decreases with decreasing flow coefficients below point (4). In particular, the bottom curve shows that the leading edge flow spillage below the blade tip starts to increase from near zero at the equilibrium solution limit (point (4)). The onset of tip clearance flow

spillage below the blade tip means that the incoming/flow tip clearance flow interface crosses the leading edge blade tip. This is the flow feature identified in chapter 2.

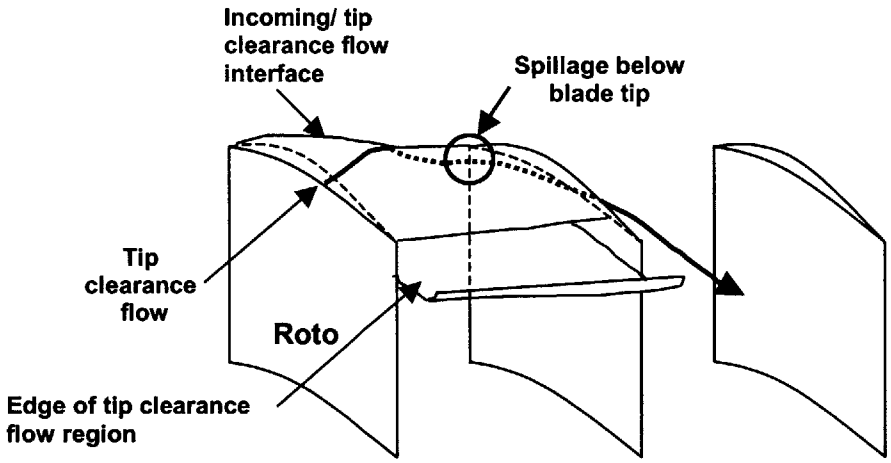

Figure 3.8. Leading edge tip clearance flow spillage below blade tip

Figure 3.9. Mass flow through blade tip and spilled ahead of leading edge below blade tip (1.8% chord tip clearance)

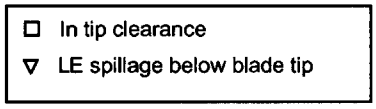

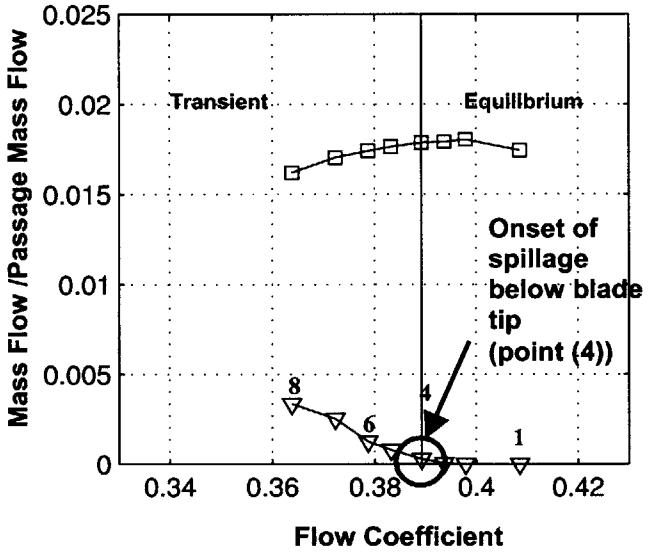

In sections 3.2.3 and 3.2.4, we will explain how the above threshold flow events set the equilibrium solution limit and contribute to the observed blockage growth.

3.2.3 Trailing Edge Backflow Below Blade Tip

Figure 3.6 shows that the backflow of tip clearance fluid from adjacent blade passages impinges on the pressure surface. Figure 3.10 explains how this impingement

leads to additional backflow and an increase of the tip clearance blockage. The flow features of interest are marked with red circles.

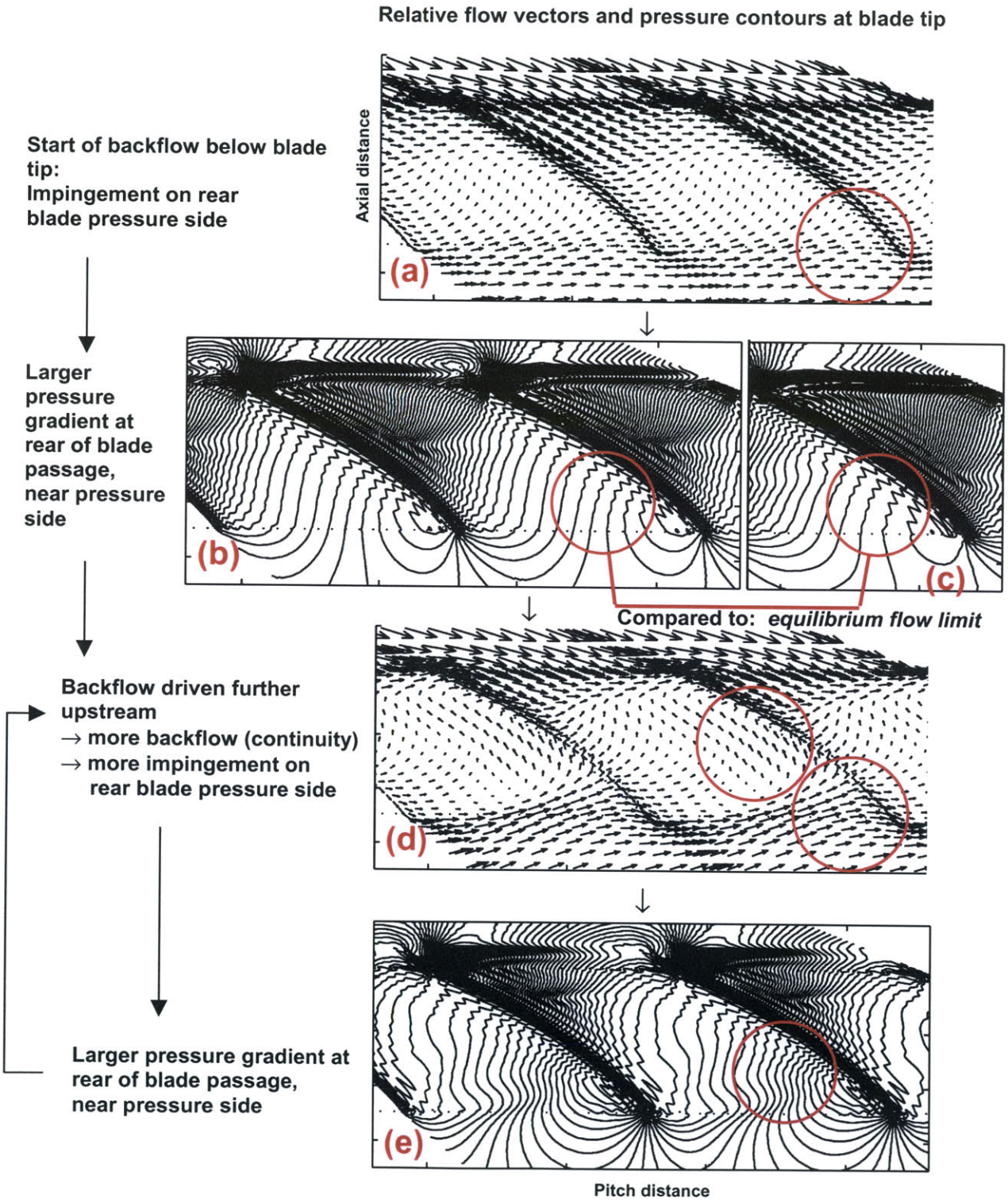

Figure 3.10. Role of tip clearance backflow below the blade tip on equilibrium flow limit

At the equilibrium solution limit, there is no average backflow below the blade tip at the trailing edge as mentioned earlier. When the back pressure is increased, backflow starts. The impingement of the backflow on the pressure surface (figure 3.10a) increases the local pressure gradient at the rear of the blade passage, as shown by the tighter static pressure contours (figure 3.10b) compared to those at the equilibrium flow limit (figure 3.10c), driving the backflow upstream (figure 3.10d). Most of the impinged backflow move upstream toward the passage inlet because the blade passage is a diffuser and the pressure at the exit is higher than at the inlet. By continuity, the movement of this fluid upstream towards the leading edge leads to enhancement in backflow (figure 3.10d) and thus more local pressure rise from impingement (figure 3.10e).

Tip clearance backflow accounts for the increase in tip blockage seen past the equilibrium solution limit. Figure 3.11 shows the variation with flow coefficient of the tip blockage, the contribution from backflow (regions of negative axial velocity) and the contribution from local tip clearance fluid (*tip blockage - backflow blockage*) for the 1.8% tip clearance case of figure 3.4. In the transient flow regime beyond the equilibrium flow limit, between points (4) and (8), the rate of increase in blockage associated with backflow with respect to flow coefficient accounts for most of the rate of increase in tip blockage.

Figure 3.11. Contribution of tip clearance backflow to tip blockage

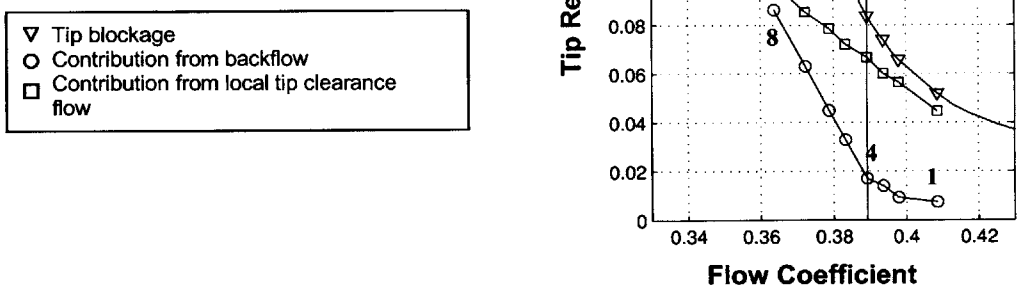

Tip clearance backflow is also responsible for the increase in blockage from local tip clearance fluid. To understand this, one must first review the blockage generation

mechanism of tip clearance flow in compressors. Khalid [17] modeled the flow exiting the tip clearance gap as a series of wakes along the blade chord because its relative stagnation pressure is lower than that of the incoming fluid. As these wakes convect up the passage pressure gradient towards to exit plane, their blockage increases. Thus, the lower the relative stagnation pressure of the wake and/or the larger the pressure rise it experiences (i.e. the nearer the wake is to the leading edge of the rotor) the higher the blockage generation will be. In this case, figure 3.12 shows that the backflow displaces the local tip clearance fluid toward the leading edge, where pressure rise to the passage exit plane is the greatest. This fluid has low relative stagnation pressure and as it leaks through the adjacent tip clearance gap near the leading edge, it generates more blockage in the next blade passage than if it were distributed equally along the blade chord (in the absence of backflow), in which case it would experience a lower pressure rise as it convects downstream in the adjacent blade passage.

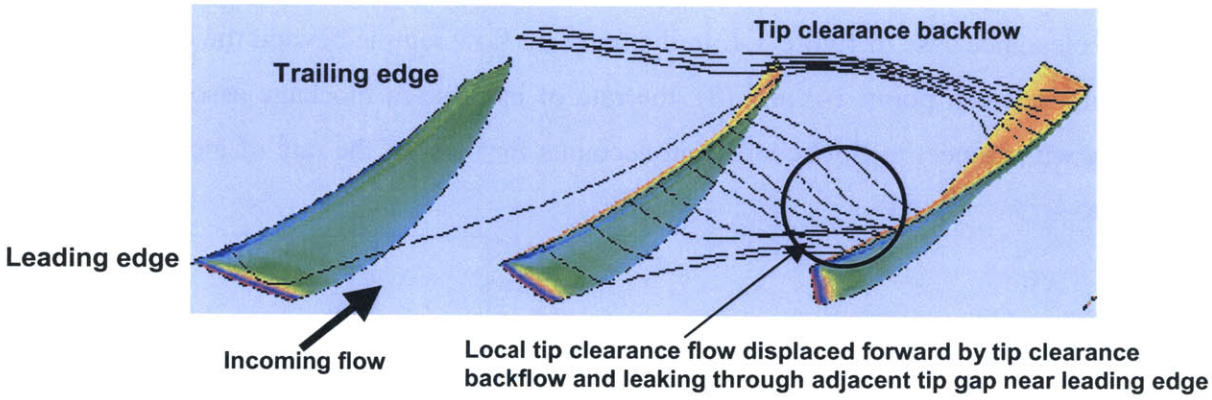

Figure 3.12. Indirect contribution of tip clearance backflow to tip blockage

3.2.4 Leading Edge Spillage Below Blade Tip

In this section, we will explain how the second threshold flow event, leading edge tip clearance fluid spillage below the blade tip, allows the tip clearance backflow to move upstream. Figure 3.13 displays the relative stagnation pressure deficiency (with respect to the incoming flow) of the tip clearance fluid that flow through the adjacent blade tip clearance gap versus that of the tip clearance fluid that spills ahead of the adjacent blade leading edge for point (6) in figure 3.9. This figure points out that the tip clearance fluid

that spills below the adjacent leading edge blade tip has lower relative stagnation pressure loss than if it had to leak through the adjacent tip clearance gap.

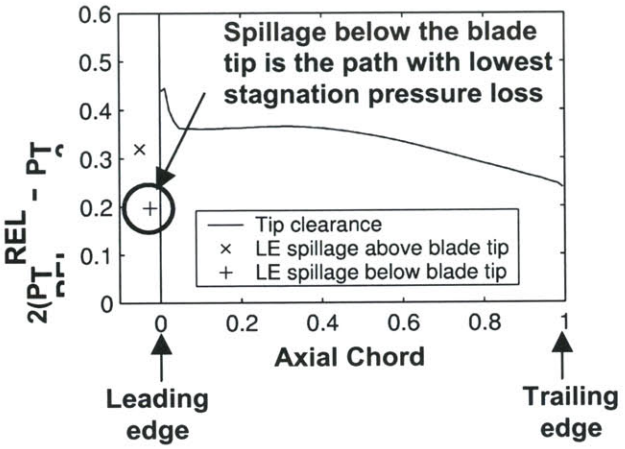

Figure 3.13. Relative stagnation pressure deficiency (loss) of fluid flowing through the tip clearance gap and fluid spilled ahead of the leading edge for point (6) in figure 3.9

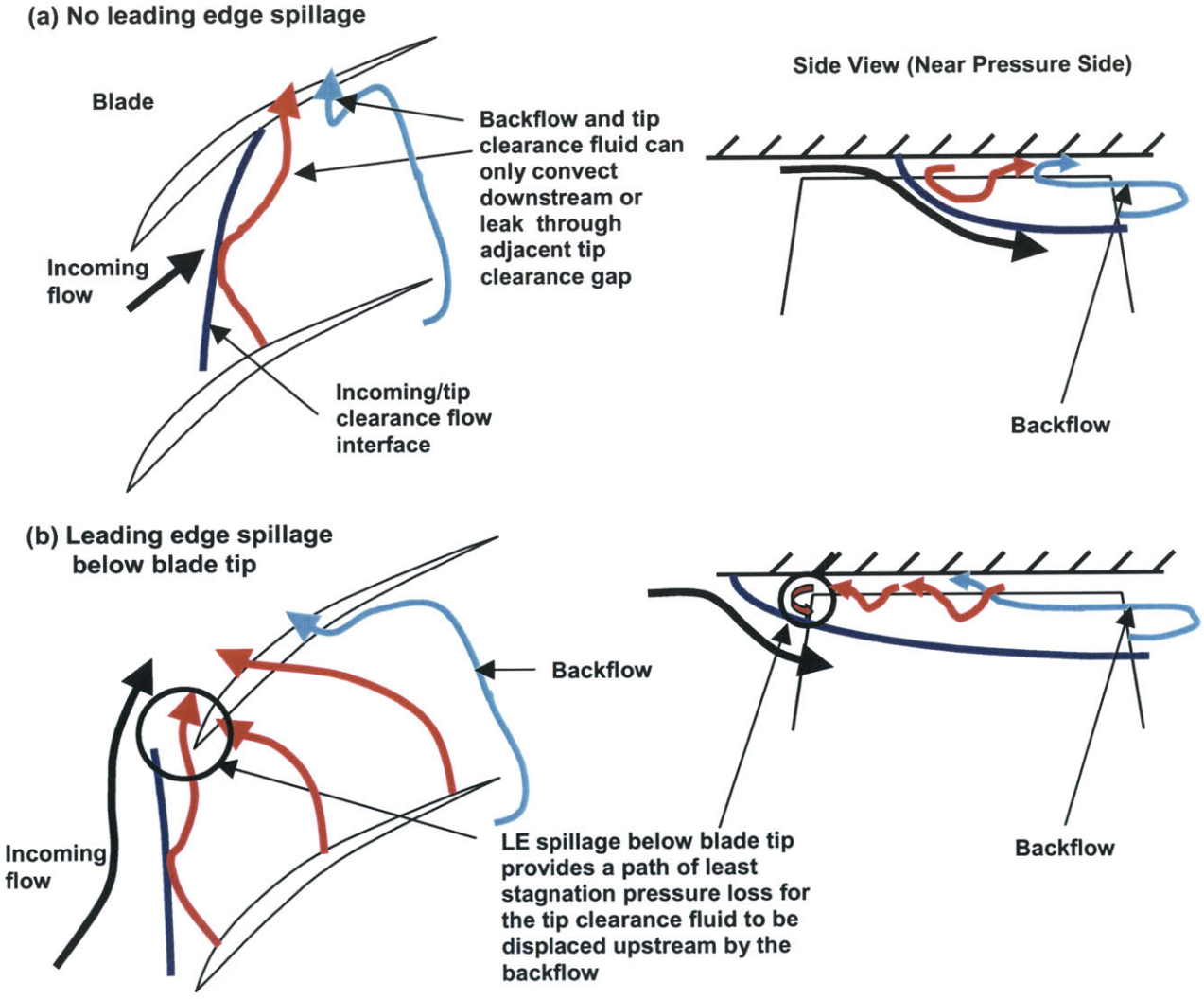

Figure 3.14. Role of leading edge spillage below blade tip on upstream propagation of backflow

Figure 3.14 shows the significance of the path of low stagnation pressure loss provided by leading edge flow spillage below the blade tip. When the incoming/tip clearance flow interface is inside the blade passage (no leading edge spillage) (figure 3.14a) the tip clearance fluid and backflow fluid cannot propagate upstream because the interaction with incoming flow redirects them downstream or through the adjacent tip clearance gap. On the other hand, the presence of leading edge spillage below the blade tip (figure 3.14b) provides a path of lower resistance than going through the adjacent tip gap for the tip clearance fluid (analogous to flow through an open pipe versus flow through an orifice), such that this fluid can be displaced upstream by the backflow.

3.2.5 Criteria for Blade Passage Equilibrium Flow Limit

From the discussion on threshold flow events presented in sections 3.2.2 through 3.2.4 the two criteria that set the blade passage equilibrium solution limit are:

(1) Zero pitch-averaged mass flow across the pitch at the trailing edge blade tip (onset of tip clearance backflow), as shown by points (4) in figure 3.7

(2) Onset of leading edge tip clearance flow spillage below the blade tip, as shown by points (4) in figure 3.9

Although the threshold flow events may start at different flow coefficients, both must be present (i.e. both criteria must be satisfied) for the equilibrium solution limit to be reached. In other words, the equilibrium flow limit occurs at the lower of the two flow coefficients where each threshold flow event starts to occur.

For example, tip clearance backflow can start at a higher flow coefficient than leading edge spillage, but the equilibrium limit will only occur when the latter event come about. This is demonstrated by the E3 rotor B computations at 3.0% chord tip clearance. The time-averaged speedline, pitch-averaged mass flow and spillage mass flow distributions for this case are presented in figures 3.15a, b and c, respectively. Figure 3.15b shows that backflow below the blade tip starts at point (1) but the equilibrium flow limit does not occur until the onset of leading edge spillage below the blade tip at point

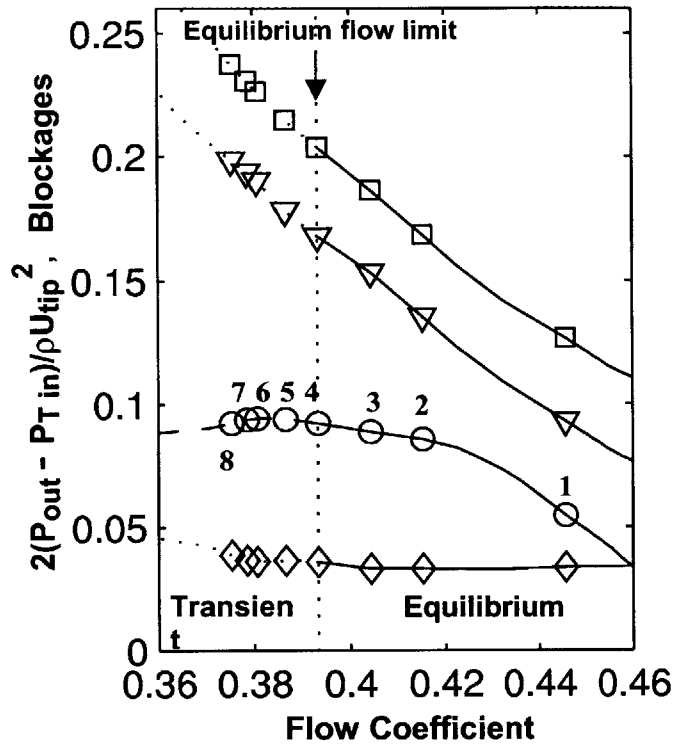

(a) Speedline , blockages

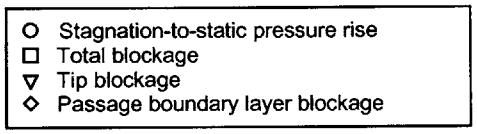

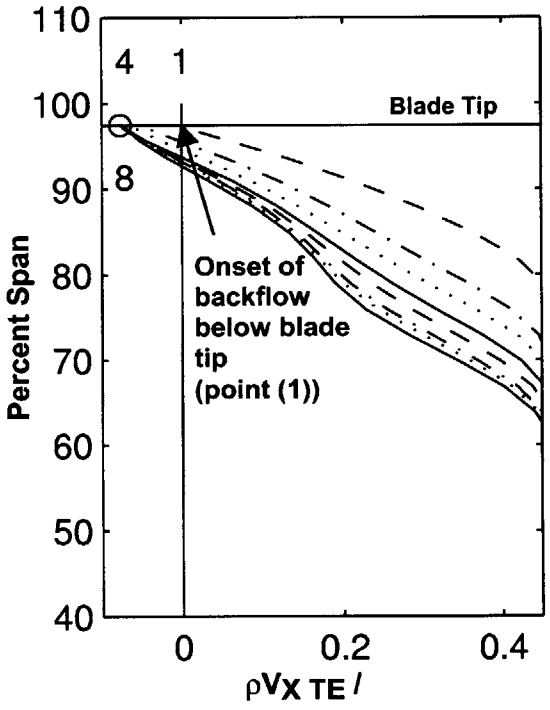

(b) Spanwise distribution of pitch-averaged mass flow at passage exit plane

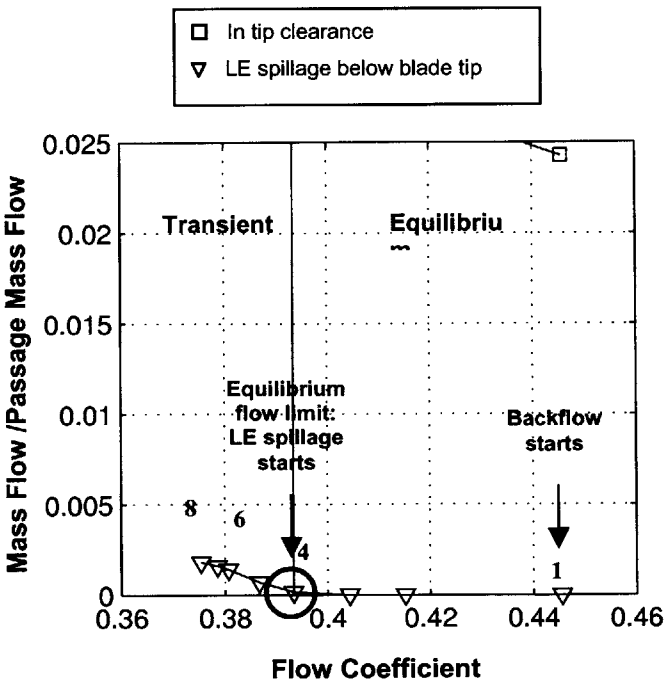

(c) Mass flow through blade tip and spilled ahead of leading edge below blade tip

Figure 3.15. Evaluation of passage equilibrium flow limit criteria for 3.0% chord tip clearance

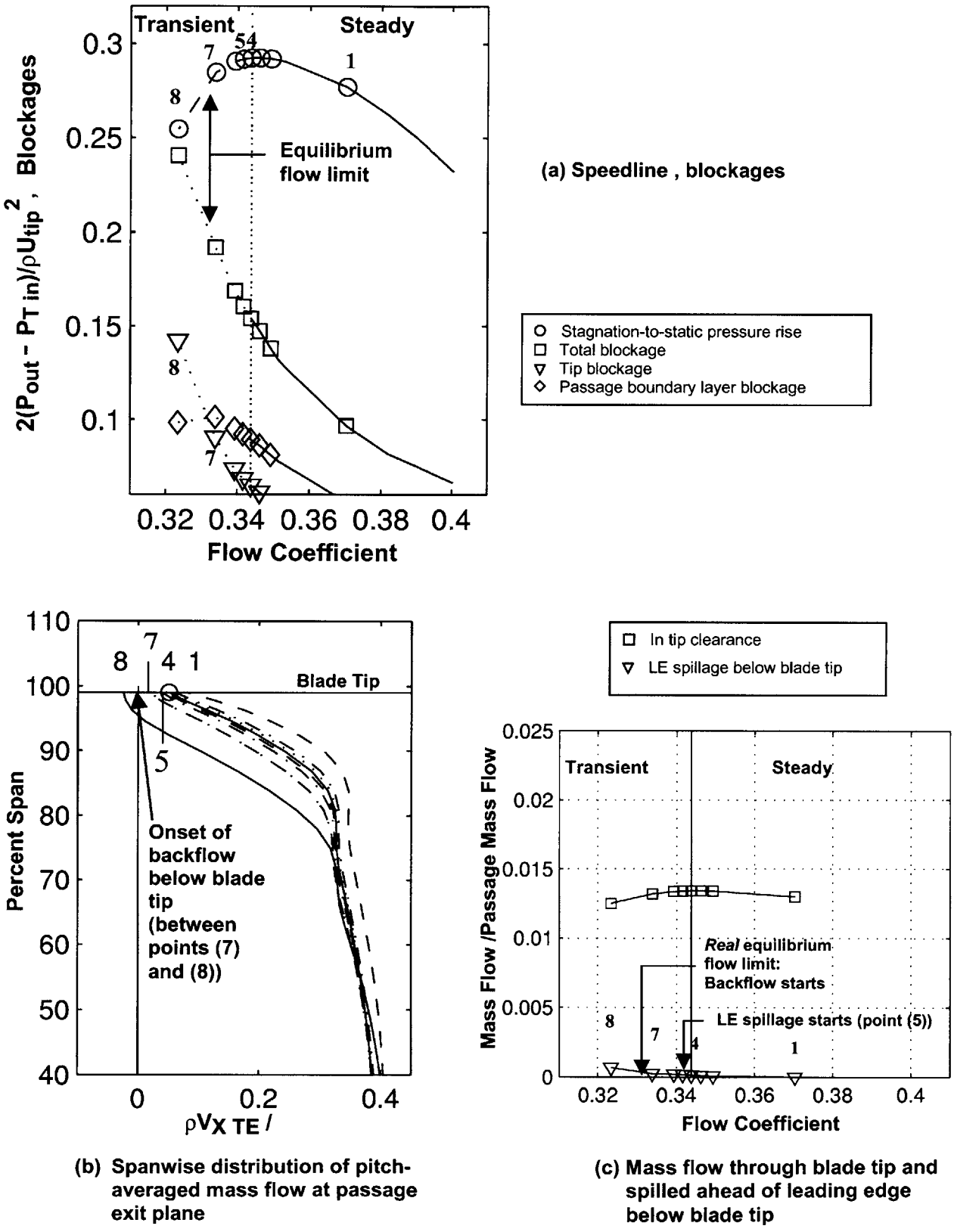

Figure 3.16. Evaluation of passage equilibrium flow limit criteria for 1.2% chord tip clearance

(4) (figure 3.15c).

In the opposite case, the leading edge spillage may occur at a higher flow coefficient than the backflow, but equilibrium flow limit is reached when backflow below the blade tip comes about. As an example, figure 3.16 presents the same information as figure 3.15 for 1.2% chord tip clearance. Figure 3.16b shows that the leading edge spillage below the blade tip occurs first at point (5). However, tip clearance backflow does not happen until the mass flow reaches a value between points (7) and (8). It is only between points (7) and (8) in figure 3.16a where the equilibrium solution limit is reached, as characterized by the growth in tip blockage versus the leveling of passage boundary layer blockage.

Moreover, the 1.2% tip clearance case also demonstrates the importance of the exit boundary condition in capturing the equilibrium flow limit in a single blade passage computation run in steady mode. In this case, the equilibrium flow limit (between points (7) and (8)) lies in the transient flow regime (mass flow lower than point (4)) and will not be captured by a steady computation. The steady solution limit is reached at point (4) in figure 3.16a because the exit static pressure boundary condition used cannot handle the pressure rise turnover at flow coefficients below point (4). An alternative exit boundary condition, e.g. downstream stator or throttle, should allow the equilibrium passage flow limit to match the steady solution limit.

3.3 Summary

The link between the single passage equilibrium flow limit and tip clearance flow can be summarized as follows:

- The equilibrium solution limit is characterized by the onset of growth of the passage tip blockage without settling to a new equilibrium value until the tip blockage grows to the hub.

- The onset of this growth in tip blockage is marked by two threshold flow events that can start at different flow coefficients but must both be present:

(1) The backflow of tip clearance fluid from adjacent blade passages at the trailing edge plane below the blade tip, which impinges in the blade pressure side

(2) The spillage of tip clearance fluid ahead of the blade leading edge below the blade tip into the next passage.

In the next chapter we connect the above description of the blade passage equilibrium flow limit with the formation of spike disturbances. This link can be predicted based on four factors:

(1) The phenomena described occur in the tip region, where spike disturbances have been experimentally detected.

(2) The phenomena rely on the spillage of tip clearance fluid to the adjacent blade passage ahead of the rotor leading edge. This is consistent with the generic flow feature identified in chapter 2, where the incoming/tip clearance flow interface lines up with the rotor leading edge plane for spike stall inception.

(3) We have observed the impingement pattern of trailing edge backflow in the stall computations by Hah *et al.* [13] on another low-speed rotor geometry.

(4) The required presence of both threshold flow events for stall inception can be observed in the study of rotating instabilities by Marz *et al.* [22]. Trailing edge backflow can been seen in their multiple blade passage computations in the stable flow range, but they claim that stall did not occur until the tip clearance flow leaks across the blade leading edge.

Chapter 4

Link to Stall Inception

The computational study in chapter 3 revealed that a combination of trailing edge backflow of tip clearance fluid and leading edge spillage of tip clearance flow sets the equilibrium flow limit. Criteria associated with this limiting behavior of the tip clearance flow on passage flow equilibrium were proposed. To link the proposed criteria to stall inception, multiple blade passage computations are performed to show that the criteria that set the single blade passage equilibrium flow limit lead to the formation of spike disturbances. The proposed mechanism for spike formation is assessed for consistency with published experimental observations on stall inception.

4.1 Formation of Spike Disturbances

In section 3.2.1, the similarity in single passage flow transient past the equilibrium solution limit was mentioned for all the computed tip clearance sizes. Similarity in stall inception behavior can hence be implied and one stall simulation is sufficient. The tip clearance size selected for the stall inception simulation is 1.8% chord for the same reasons described in section 3.2.1, namely a negative slope of the stagnation-to-static pressure rise characteristics at the equilibrium flow limit and the absence of tip clearance flow oscillations. Although a full annulus stall inception simulation would be ideal in order to capture all the harmonics of modal stall inception, the number of blade passages had to be kept to a minimum to keep the mesh size and simulation time reasonable

(appendix C). Six blade passages are considered sufficient to simulate the formation of spike stall disturbances in this case because:

- The slope of the total-to-static pressure rise characteristics at the equilibrium flow limit is negative in this case, excluding modal stall inception

- Spike disturbances have been experimentally measured to have a circumferential extent of two to three blade passages ([4], [5], [8], [16], [27])

The computational procedure used the single blade passage mesh of chapter 3, which involves increasing the exit pressure beyond the value at the equilibrium solution limit by 0.08% of the dynamic head based on blade tip speed. The single blade passage equilibrium solution limit was taken as the initial flow condition. It is noted that the single blade passage equilibrium flow limit also represents the equilibrium flow (limit) condition in the multiple blade passage blade passage environment since every blade passage is the same. Thus, we are not prejudicing the multiple blade passage results by using the single blade passage equilibrium solution limit. Its use as an initial flow condition saves computational time since one does not have to recompute the equilibrium flow limit for the multiple blade passage configuration. The equivalence between single and multiple blade passage equilibrium limit is evidenced by the fact that in the absence of any introduced asymmetry in the flow field, all blade passages stall simultaneously with the same flow transient beyond the equilibrium solution limit as the single blade passage computation. Circumferential asymmetry must therefore be introduced into the flow field in the form of a disturbance six blade passages in wavelength over the full span (i.e. similar to a modal disturbance) in order not to favor the tip region and consequently prejudicing the results toward spike stall inception. It was applied only during the first ten blade-pitch convection times (or blade passing times [*BPT*]) and removed long before the formation of the spike disturbance. The computational code, mesh and procedure used are described in detail in appendix C.

Figure 4.1 shows the results for the multiple blade passage stall simulation. The first plot displays the time history of the mass flow. The latter plots show the deviation

from the passage-averaged axial velocity distribution, normalized by the blade tip velocity, at different times (marked in the mass flow time history) during the stall transient. Hot-wires used in stall inception experiments measure this velocity deviations, albeit at only one radial location. The axial position chosen for the plots is 18% chord upstream of the rotor leading edge. This is representative of hot-wire locations used to measure spike disturbances ([4], [27]).

At time (1), when the initially imposed inlet stagnation pressure disturbance is removed, no visible velocity defect at the blade tip is seen, showing that the introduced flow asymmetry did not bias the results in favor of spikes. A short length-scale disturbance (in the form of an axial velocity deviation near the casing that is more pronounced at the crest than the peak of the wave) appears at time (3), accompanied by a rapid drop in the mass flow. A velocity defect near the casing and extending over two to three blade pitches becomes visible. The disturbance grows rapidly in amplitude and spreads toward the hub, as seen at time (4). It becomes more two-dimensional at time (5), covering the fundamental harmonic of the six-blade domain.

On the axial velocity deviation plots, the blades rotate from left to right along the *theta/pitch* axis. The velocity defect (short length-scale disturbance) rotates in the reverse direction (with respect to the blades) since it rotates slower than the rotor in the absolute frame of reference. The location of the peak of the short length-scale disturbance at different time steps allows estimation of the rotational velocity of the disturbance. The peak of the velocity defect has moved by about 3 blade pitches between time steps (3) and (4), which are 10 blade passing times (*BPT*) apart, and the speed of the disturbance is thus about 70% of the rotor speed. The time to grow into fully developed stall can be estimated by the time it takes for the disturbance from inception (~time (3)) to extend across the entire span (~time (5)), which is about two rotor revolutions.

Table 4.1 compares the computed short length-scale disturbance to the experimentally measured spike disturbance in front of the E3 rotor B obtained from hot-wire traces [27] as summarized by Gong *et al.* [11]. The disturbance obtained from the computations compares well with the measured features. However, because the length-scale of the computed disturbance (two-to-three blade passages) covers about half of the fundamental wavelength of the domain (six blade passages), computations with more

blade passages should be pursued to ensure that the number of passages used in the computation have no influence on the resulting disturbance

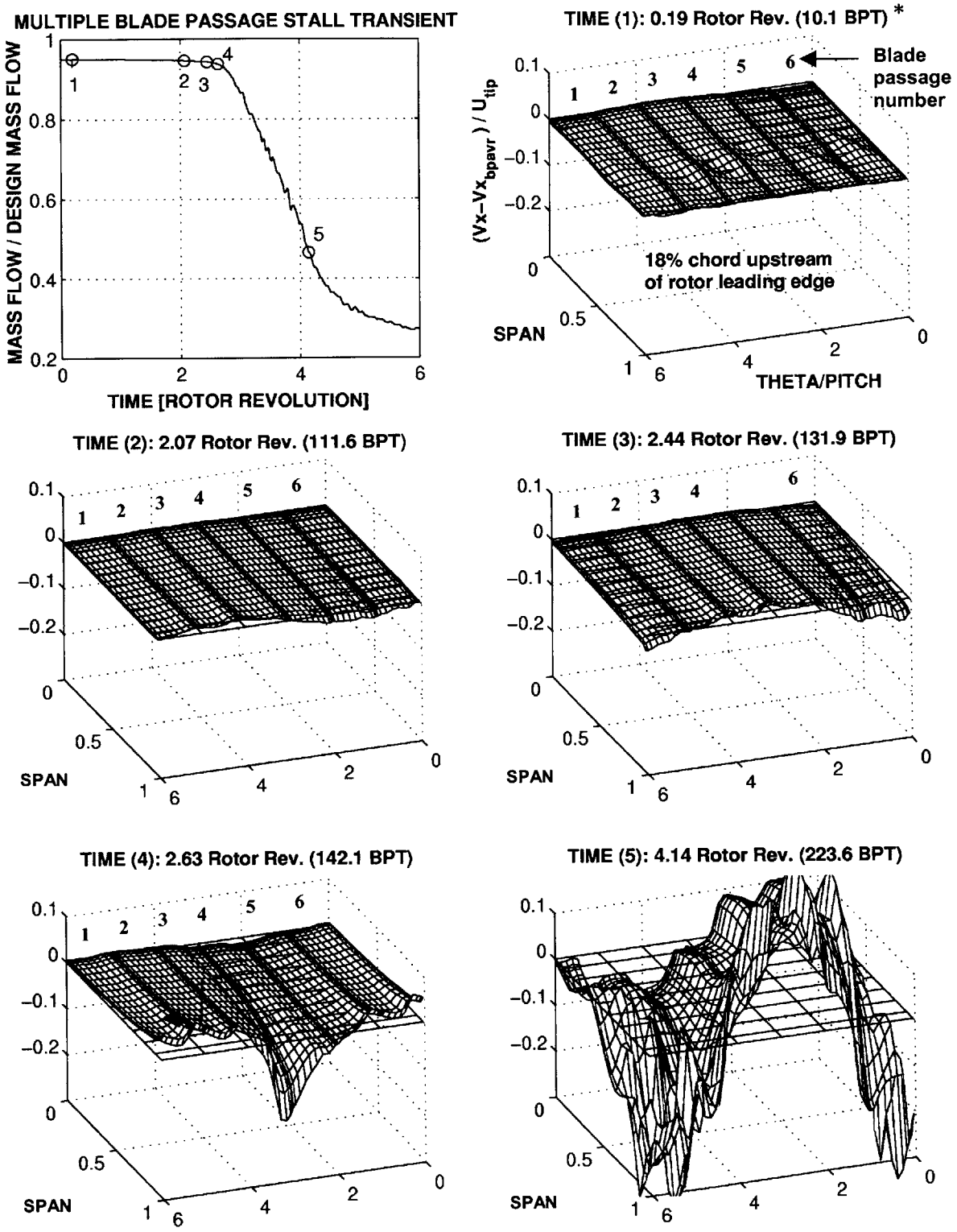

Figure 4.1 Stall transient for multiple (6) blade passage configuration (* *BPT*=blade passing time)

. Table 4.1. Comparison of measured ([11], [27]) and computed spike disturbance

Characteristics	Experiment	Computation
Circumferential Extent	~2-3 blade pitch	~2-3 blade pitch
Radial Extent	concentrated in tip region	last 10-20% span
Rotating Speed	70-73% of rotor speed	~70% of rotor speed
Growth Time to Full Stall Cell	~3 rotor revolutions	~2 rotor revolutions

The next step is to verify that the scenario for the formation of the spike disturbance is consistent with that behind the single blade passage equilibrium flow limit. This is done by observing the tip clearance flow behavior, in terms of tip clearance backflow at the trailing edge and leading edge tip clearance fluid spillage, for the blade passage behind the spike disturbance.

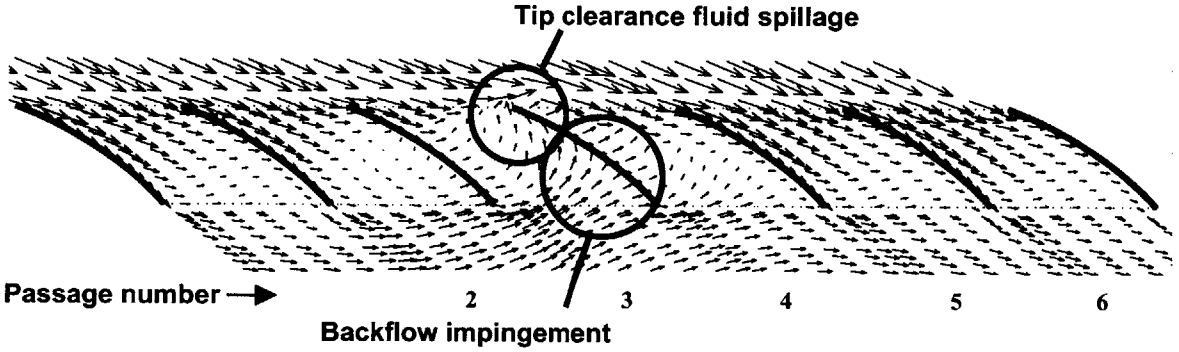

Figure 4.2. Relative flow vectors at blade tip at time (4)

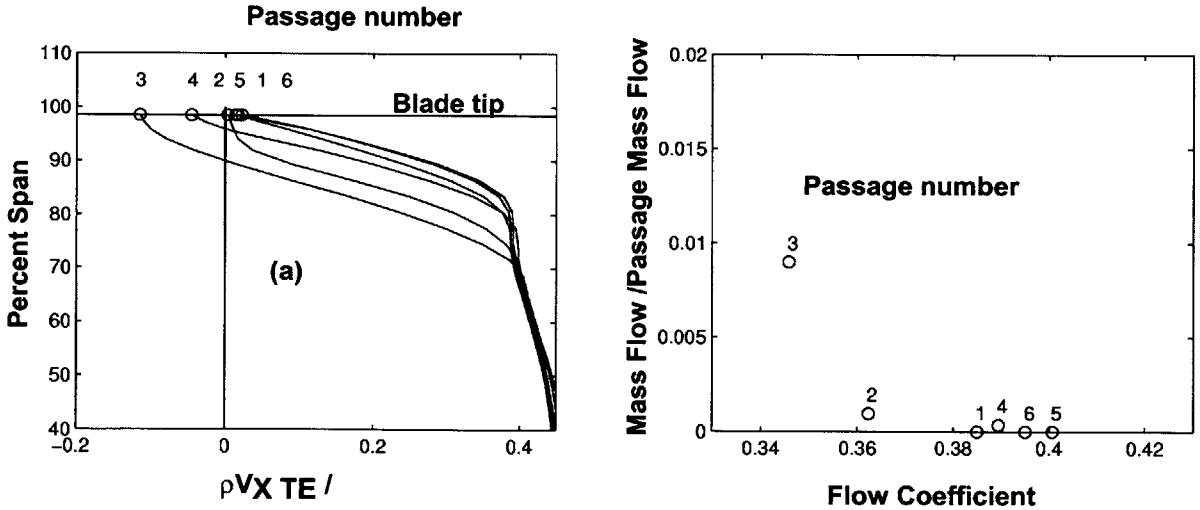

(a) Spanwise distribution of pitch-averaged mass flow at passage exit plane

(b) Leading edge spillage of tip clearance fluid below the blade tip

Figure 4.3. Tip clearance flow behavior in each blade passage at time (4)

Figure 4.2 displays the relative flow vectors at the blade tip radius at time (4). At this time the velocity defect (spike disturbance) is in front of blade passages 3 and 4 and is moving towards blade passage 5. Figures 4.3 show the corresponding spanwise distribution of pitch-averaged mass flow and leading edge tip clearance fluid spillage below the blade tip, for each blade passage. From figures 4.2 and 4.3a, passages 3 and 4 show trailing edge backflow and impingement below the blade tip due to tip clearance fluid from adjacent blade passages. The other blade passages do not exhibit any trailing edge backflow below the blade tip. Figures 4.2 and 4.3b also show leading edge spillage of tip clearance fluid below the blade tip from blade passage (3) into passage (4). These two flow events are similar in nature, if not in quantity, to those observed in the single blade passage flow transient past the equilibrium solution limit, for which the blade-to-blade periodic condition is no longer valid in the computed multiple blade passage flow. However, it is to be noted that under the conditions that the computational experiments have been carried out, the flow computed in a single blade passage and in the multiple blade passage is identical up to the equilibrium solution limit.

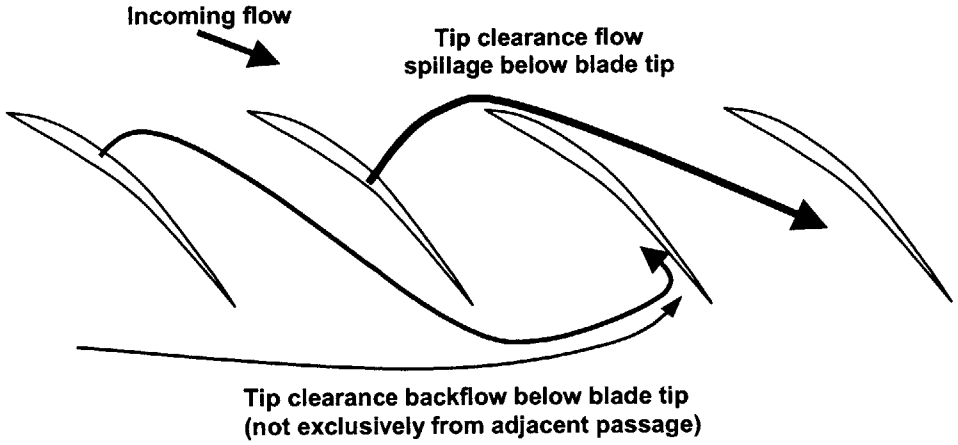

Figure 4.4. Simultaneous flow events in spike formation and length-scale of spike disturbance

Moreover, the two flow events set the length-scale of the spike disturbance at two-to-three blade pitches as depicted in figure 4.4, where a minimum of three blade passages are involved. All the leading edge spillage fluid from the middle passage flows into the next one, such that the disturbance is most pronounced for these two passages. The backflow tip clearance fluid may come mainly from the left blade passage, but also from one or two passages beyond. This means that the effect of backflow on the disturbance is

distributed among several passages and thus not as pronounced for the left passage as is the effect of spillage on the disturbance for the right passage. This explains why the length-scale is two-to-three blade pitches and not simply three. For the computation shown in figures 4.2 and 4.3, the length-scale of the spike is set by tip clearance fluid spillage from passages (3) into (4) and the trailing edge backflow of tip clearance fluid from passages (2) and (1) into passage (3). This length-scale concurs with that of spikes measured in experiments on different compressors ([4], [5], [8], [16], [27]).

From the multiple blade passage stall simulation and analysis, it is seen that the criteria that set the single blade passage equilibrium flow limit lead to the formation of spike stall disturbances. The single blade passage equilibrium flow limit thus corresponds to the onset of spike disturbances. It must be noted that the equilibrium solution limit is a sufficient condition for spike formation but not a necessary one since a disturbance of sufficient amplitude introduced a higher mass flow could trigger spike formation. However, even in this case the proposed spike formation scenario in terms tip clearance backflow and spillage should still apply. In addition, the two criteria involved in the spike formation process explain the observed length-scale of spike disturbances of two-to-three blade passages.

4.2 Consistency With Stall Inception Experiments

In this section, the proposed scenario for spike formation is assessed for consistency with published observations.

4.2.1 Optimal Measurement Location For Spike disturbances

Park [25] observed that the best place to detect the spike disturbance on the E3 compressor was at the trailing edge of the first rotor near the casing, using either casing pressure sensor or hot-wires. This is also reflected in the multiple blade passage computation. Figure 4.5a repeats the axial velocity deviation at 18% chord upstream of the rotor leading edge, taken at time (4) in figure 4.1. Figure 4.5b shows the corresponding axial velocity deviation taken at 20% chord downstream of the rotor

trailing edge and shows a more pronounced velocity defect. The explanation based on the proposed spike formation scenario is that trailing edge backflow below the blade tip of tip clearance fluid from adjacent blade passages is the initiator in the formation of spike disturbances.

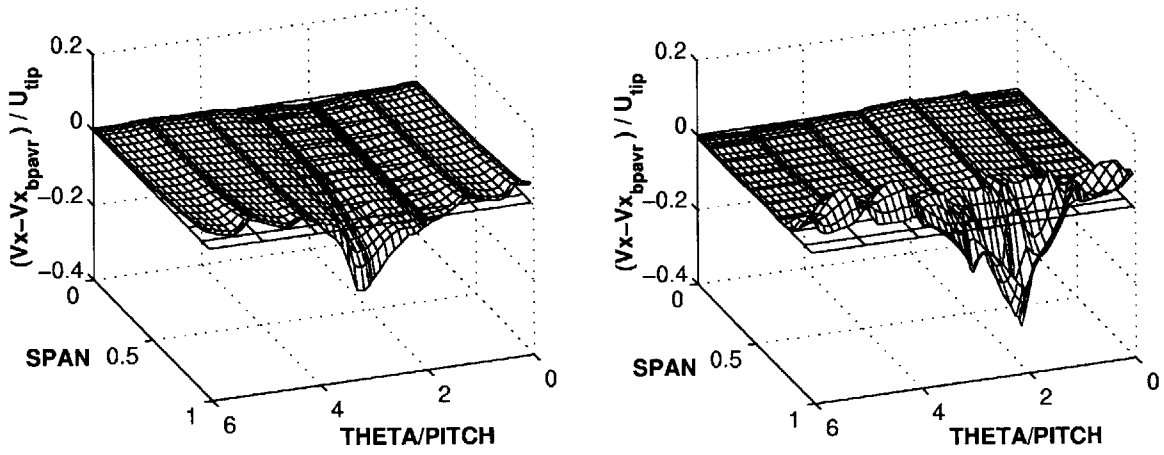

(a) 18% chord upstream of leading edge **(b) 20% chord downstream of trailing edge**

Figure 4.5. Axial velocity deviation at different axial location at time (4) in figure 4.1

4.2.2 Critical Incidence Theory

Camp *et al.* [2] observed through variation of IGV angles that spike stall inception seem to occur at a particular value of tip incidence, termed "critical incidence". The tip incidence was estimated from mass flow and velocity triangles. As shown in figure 4.6, for cases exhibiting spike stall inception, the tip incidences all fall within a range of less than one degree. In contrast, the variation in tip incidence was more than several degrees for cases exhibiting modal stall inception.

From the E3 rotor B computations in chapter 3, it will be shown that the "critical tip incidence" is the blade loading at which both the backflow and spillage criteria for spike formation is satisfied. For Camp *et al.* [2], the mass flow at which this blade loading occurs changes because the inlet guide vanes stagger angle, and thus the first rotor velocity triangles, was changed. In our case, with only the tip clearance size changing, the mass flow at which the spike formation criteria are satisfied is about the same for cases where the tip clearance flow dominates in terms of blockage. The stagnation-to-static

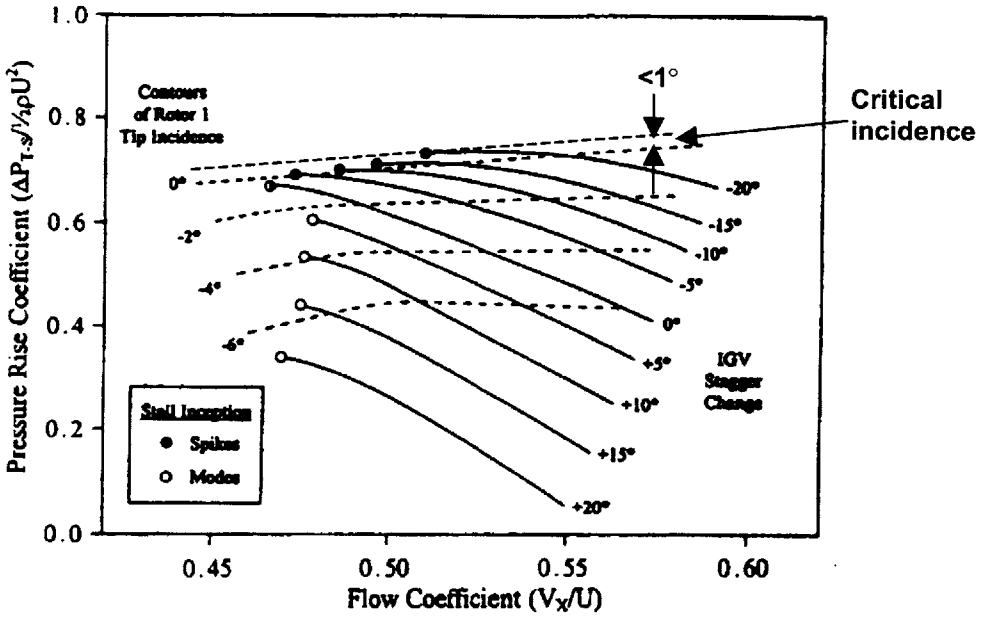

Figure 4.6. First stage stagnation-to-static pressure rise for four-stage compressor showing stall inception type and corresponding first rotor incidence [2].

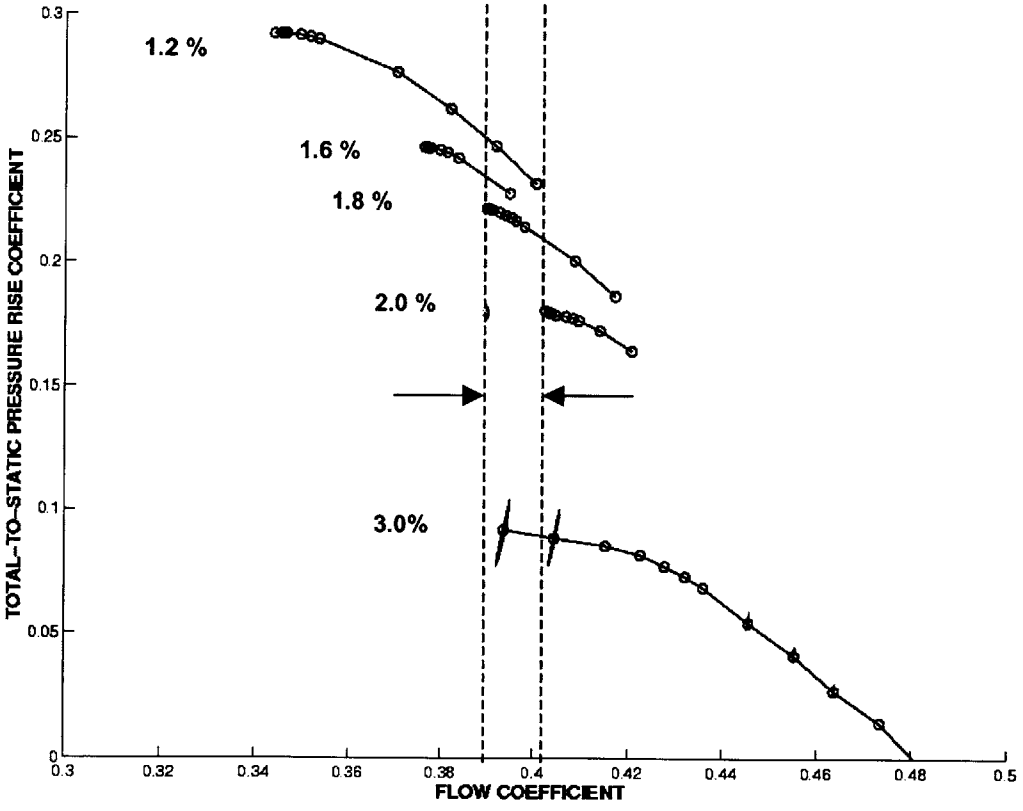

Figure 4.7. Computed stagnation-to-static pressure rise characteristic across E3 rotor B at different tip clearances (% chord) (repeated from figure 3.2)

pressure rise characteristics in figure 4.7 (repeated from figure 3.2) shows that for tip clearance sizes of 1.8% chord and above, spike formation occurs at a flow coefficient in the 0.39-0.40 range. Figure 4.8 plots the corresponding tip incidence versus flow coefficient. The incidence is estimated from mass flow and velocity triangles as done by Day *et al.* [2]. For the 0.39-0.40 range of flow coefficient, the tip incidence would fall within 0.5 degree, and is thus consistent with the "critical tip incidence" observation.

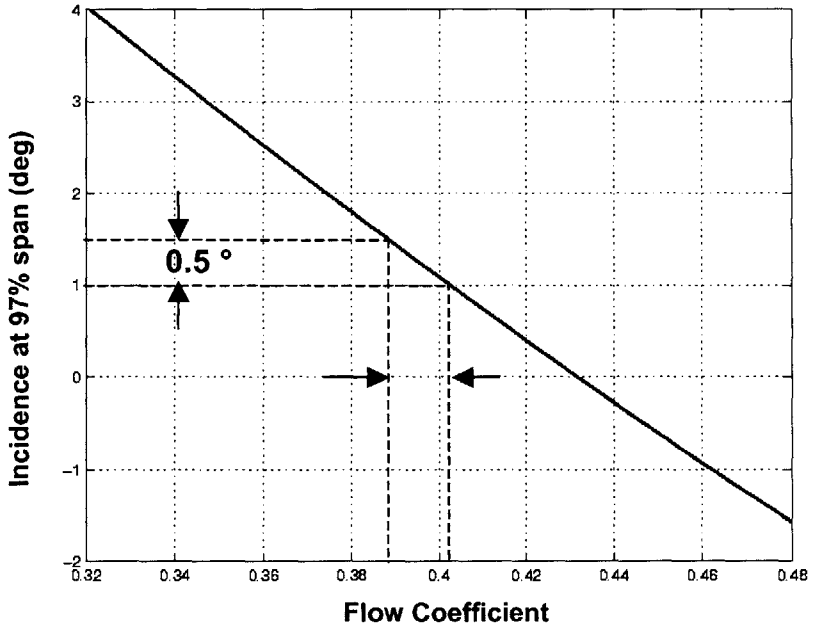

Figure 4.8. E3 rotor B tip incidence versus flow coefficient

The E3 rotor B cases with tip clearance size of 1.8% chord and above have their blockage increase with decreasing flow coefficient due *almost entirely to tip clearance flow* rather than from the passage boundary layer, as shown in figures 3.4a and 3.15a from the relative slopes of the tip and passage boundary layer blockage curves prior to the equilibrium flow limit (points (1) through (4)). In addition, figures 3.9 and 3.15c also show that the equilibrium flow limit is reached when leading edge tip clearance flow spillage occurs. This means that the incoming/tip clearance flow interface reaches the leading edge at the blade tip at approximately the same flow coefficient for all these tip clearance sizes. This can be expected because the incoming/tip clearance flow interface trajectory is determined by the chordwise tip clearance flow distribution. In all these

cases, the lack of growth in the blade passage boundary layer implies similarity in the blade loading that drives the tip clearance flow [29].

For tip clearances below 1.8%, the equilibrium flow limit and thus the spike formation does not occur in the same range of flow coefficient. The reason is that, for these cases, tip clearance flow spillage starts at a higher flow coefficient than tip clearance backflow, as shown in figure 3.16 for 1.2% chord tip clearance. Equilibrium flow limit is therefore set by the occurrence of tip clearance backflow and not by the incoming/tip clearance flow interface reaching the leading edge plane.

4.2.3 Change of Stall Inception Type with Tip Clearance Size

Day [4] observed that as the tip clearance is increased, the stall inception type changes from spike to modal. The implication from our work is that the large tip blockage that comes with large rotor tip clearances causes the turnover of the *compressor* stagnation-to-static pressure rise (modal stall inception) at a higher flow coefficient than the point of spike formation (spike stall inception).

For example, figure 4.9a shows that for the E3 rotor B at 3.0% chord tip clearance case, the stagnation-to-static pressure rise characteristic is relatively flat near the passage equilibrium flow limit. The large tip clearance blockage responsible for this is shown by the time-averaged trailing edge streamwise velocity contours for a point in this region (figure 4.9b). The velocity triangles in figure 4.10 indicate that the low streamwise velocity from the blocked tip region that roughly covers the outer 30% of the span (figure 4.9b) results in high incidence over the same outer span region on the downstream stator. The combination of flat pressure rise in the rotor and high loading on the stator will lead to turnover of the compressor stagnation-to-static pressure rise characteristic. Consequently, modal stall inception will occur before spike formation (figure 4.9a).

Although the exact tip clearance size where the stall inception type changes may vary with compressors, the scenario described above can be expected to occur as rotor tip clearance size is increased in any compressor.

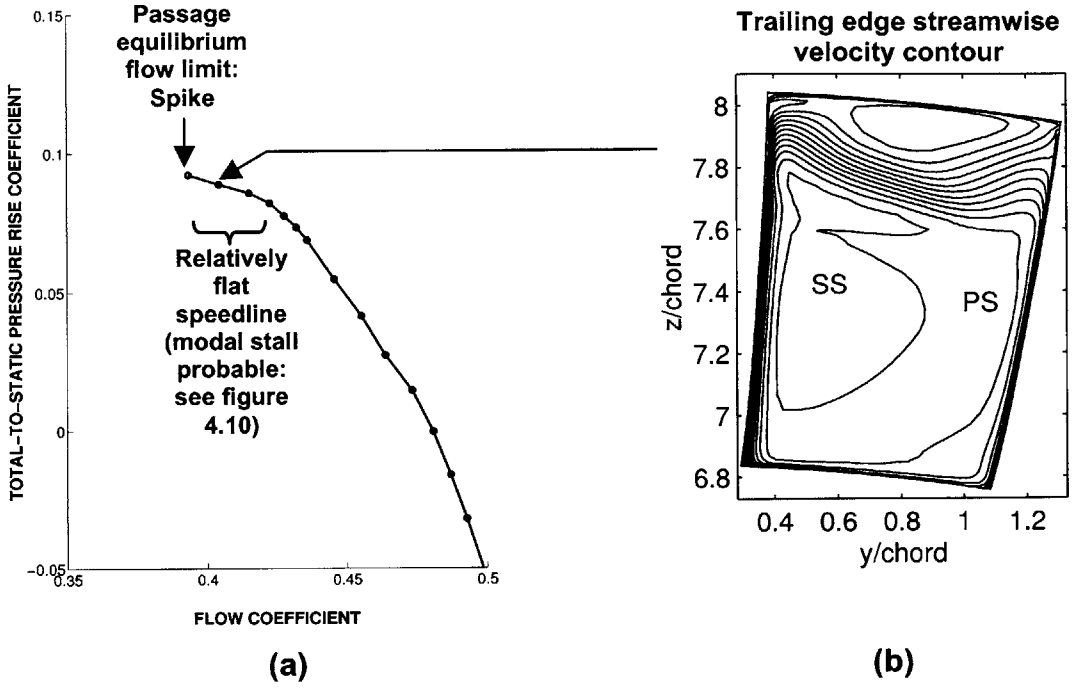

Figure 4.9. Effect of large tip clearance on rotor pressure rise (E3 Rotor B, 3.0% chord tip clearance)

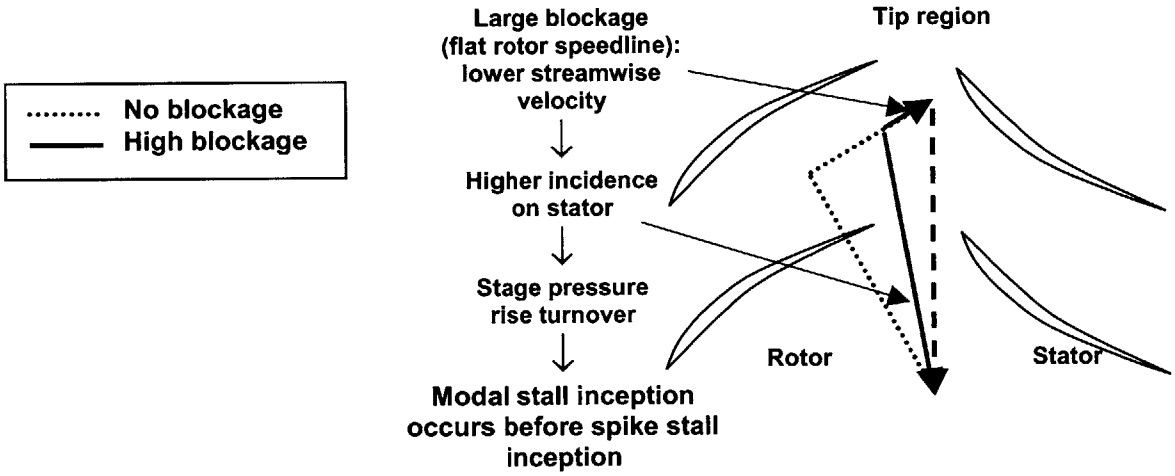

Figure 4.10. Effect of large rotor tip blockage on stator and stall inception type

4.2.4 Effectiveness of Stall Margin Improvement Strategies

Lee *et al.* [20] measured the effect of endwall suction and blowing on compressor stability. Because their work occurred prior to the discovery of either modal or spike stall

inception, no information of the stall inception type can be obtained. However, their main concern with endwall stall combined with the negative slope of the static pressure rise characteristic at stall (in the presence of endwall slots) point to spike stall inception. They reported that rear endwall suction and/or leading edge blowing, as would be associated with casing treatment, were effective in increasing stall margin. According to the proposed mechanism for spike formation, trailing edge suction of the tip clearance backflow and leading edge blowing, which would tend to delay the movement of incoming/ tip clearance flow interface to the leading edge plane, should be effective in delaying the formation of spike disturbances, and thus spike stall inception.

The view here is that any technique that delays either of the two criteria that set passage equilibrium flow limit should be effective in delaying spike stall inception. To test this hypothesis a simulation was carried out whereby the blade pitch was increased by about 30% on the E3 rotor B at 1.8% chord tip clearance. The resulting increase in surface area between the passage core flow and tip clearance flow increases the streamwise momentum transfer from the former to the latter. Thus, the movement of the incoming/tip clearance flow interface to the leading edge plane and the advent of tip clearance back flow is delayed. Figure 4.11 plots the stagnation-to-static pressure rise characteristic and blockage variation of the increased-pitch configuration versus those of the nominal configuration. The discrete points represent the equilibrium flow conditions of the increased pitch configuration, while the continuous and dashed/dotted lines show the equilibrium and transient flow conditions, respectively, of the nominal case. All blockages are normalized with the passage area of the nominal configuration for proper comparisons. It can be seen that the increase in streamwise momentum transfer from the core flow to the tip clearance flow resulted in a lower tip blockage for the high pitch case at the same flow coefficient. The equilibrium flow range was extended beyond the nominal stall point in both flow coefficient and stagnation-to-static pressure rise.

It is noted that the increase in stall margin does not contradict the trend published by Koch [19], whereby the maximum static pressure rise coefficient across the blade passage decreases with decreasing solidity. The metrics of improvement in our case are range extension in flow coefficient and stagnation-to-static pressure rise increase. However, the static pressure rise coefficient (*rotor static pressure rise from leading to trailing edge*

normalized by relative inlet dynamic head) in the increased-pitch configuration (*0.527*) is smaller than in the nominal configuration (*0.533*). The reason is that although the increased-pitch configuration gives higher maximum exit static pressure, and thus higher stagnation-to-static pressure rise, it did so at a lower mass flow. At this lower mass flow, the inlet static pressure is higher, annulling the effect of higher exit pressure on static pressure rise, and the inlet dynamic head was higher from the higher relative velocity.

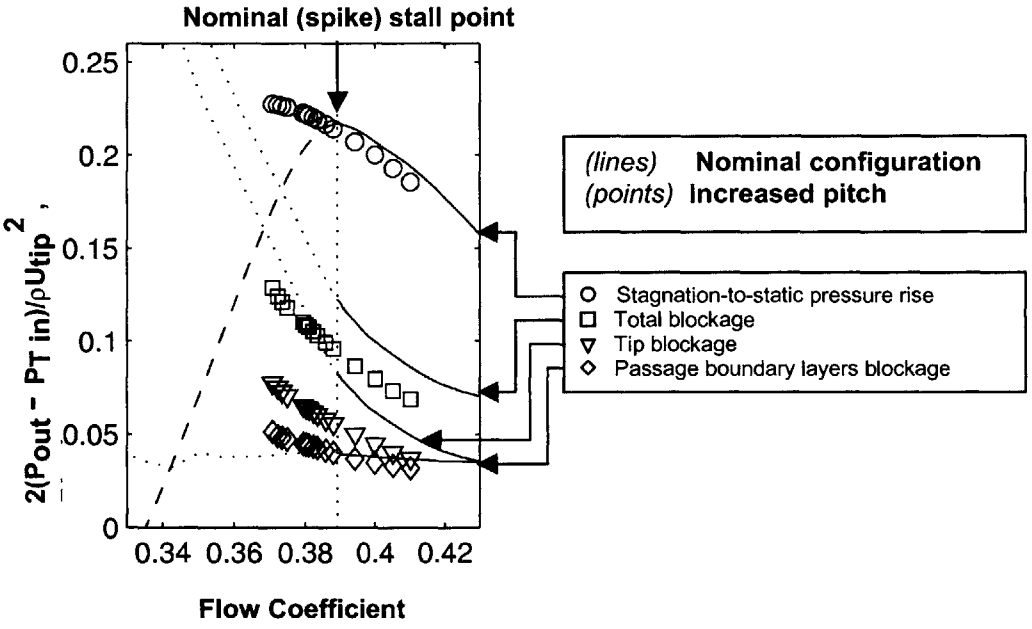

Figure 4.11. Effect of pitch increase on E3 rotor B at 1.8% chord tip clearance

4.3 Summary

Multiple blade passage computations show that spike disturbances are generated from the same flow events seen in single blade passage transients. These events are trailing edge backflow below the blade tip of tip clearance fluid from adjacent blade passages, and leading edge spillage of tip clearance fluid below the blade tip. These flow events also explain the observed length-scale of spike disturbances at two-to-three blade pitches. The criteria which apply to the single passage equilibrium flow limit also apply to the formation of spike disturbances. The proposed scenario is also consistent with the observations of axial compressor stall inception behavior.

Chapter 5

Summary, Conclusions and Recommendations for Future Work

5.1 Summary

The role of tip clearance in axial compressor stability has been assessed using time-accurate single and multiple blade passage computations. Analysis of single passage computations at and below the lowest flow coefficient for which an equilibrium solution exists enabled identification of the nature of the tip clearance flow evolution that sets this limit. The criteria associated with the limiting behavior were determined. One criterion relates to the alignment of the interface between the incoming flow and the tip clearance flow with the rotor leading edge plane. This feature is observed in other compressor rotors near the point of spike stall inception. The other criterion is the backflow of tip clearance fluid from adjacent blade passages at the trailing edge below the blade tip. Multiple blade passage computations of the formation and growth of spike disturbances show that transient tip clearance flow behavior (leading spillage, trailing edge backflow) in the development of a spike disturbance is similar in nature to that in a single blade passage environment at flows below the equilibrium solution limit.

5.2 Conclusions

The main conclusions are:

(1) The lowest flow coefficient at which an equilibrium solution exists in a single

rotor blade passage is characterized by the growth of tip clearance flow blockage until the tip blockage region reaches the hub. This onset also leads to the formation of spike disturbances in a multiple blade passage environment. It must be noted that the equilibrium solution limit is a sufficient condition for spike formation but not a necessary one since a disturbance of sufficient amplitude introduced a higher mass flow could trigger spike formation.

(2) The growth in tip blockage is caused by the impingement on the trailing edge pressure surface of backflow from tip clearance fluid of adjacent blade passages, and by leading edge spillage of tip clearance flow below the blade tip to the adjacent passage. The local increase in pressure gradient from the backflow impingement enhances the backflow. The leading edge spillage of tip clearance fluid below the adjacent blade tip provides a path with lower relative stagnation pressure loss than leakage through the adjacent tip clearance gap for the backflow to displace tip clearance fluid and propagate toward the leading edge.

(3) Zero mass flow across the pitch at the trailing edge blade tip, and the onset of leading edge tip clearance flow spillage below the blade tip (both evaluated on a time-averaged basis) form two criteria that set the lowest flow coefficient at which a single rotor blade passage can operate in equilibrium. They also signal the onset of spike disturbances. The first criterion represents the onset of tip clearance backflow below the blade tip. The second criterion translates into the trajectory of the incoming/tip clearance flow interface lining up with the rotor leading edge plane at the blade tip. The two criteria can occur at different flow coefficients but both must be present for spike disturbances to form. If the compressor stagnation-to-static pressure rise characteristic reaches zero slope at a higher flow coefficient than that satisfying both criteria, modal stall inception occurs.

(4) The two flow events associated with the proposed criteria for spike formation explain the length-scale of spike disturbances observed in our computations and in experiments.

(5) The proposed scenario for the formation of spike disturbances is consistent with published observations on stall inception behavior of axial compressors.

5.3 Implications

Implications from these results are:

(1) Features to look for in future investigations of rotating stall have been identified, namely the location of incoming/tip clearance flow interface and the presence of trailing edge backflow.

(2) For compressors that exhibit short length-scale stall inception, a flow alteration methodology that delays one of the two proposed criteria for spike formation should be successful in extending the mass flow operating range. Examples include leading edge blowing and trailing edge suction.

(3) The present work suggests that single blade passage computations may be used to predict stall inception if they have the following attributes:

- Exit flow boundary conditions that can capture equilibrium solutions past the peak pressure rise of the rotor blade passage

- Time-accurate computations so that time-averaged flow field from oscillatory equilibrium solutions can be used to evaluate the criteria for spike formation. Steady-state computations are thus not suitable for cases where unsteadiness from tip clearance flow oscillations or adjacent blade rows are present.

- Single blade passage solution for multiple blade rows to obtain the stagnation-to-static pressure rise characteristics of each blade row and of the entire compressor. This can be used to predict modal stall inception [21] and growth of spikes disturbances to fully developed rotating stall [10].

A proposed conceptual framework for the incorporation of single blade passage computations for stall prediction in a compressor design system may be contemplated as follows:

i. Carry out single blade passage computations until the equilibrium solution limit for all the blade rows in the compressor and map out the stagnation-to-static pressure rise characteristic of the compressor and of each blade row.

ii. Find the equilibrium solution limit with the highest mass flow and see if it occurs at a lower mass flow than the zero-slope peak of the *compressor* stagnation-to-static pressure rise characteristic.

iii. If yes, modal stall inception is predicted (Moore-Greitzer model [21]).

iv. If not, a spike disturbance should form in blade row with the equilibrium solution limit with the highest mass flow. To see if the spike will grow to fully developed stall at this mass flow, each blade row is replaced by body forces distributions using their respective pressure rise characteristics according to the Gong model [10] and a spike disturbance is input into the modeled system at the blade row in question.

5.4 Recommendations for Future Work

The first task is to ascertain that the number of passages (six) used in the multiple blade passage computation of section 4.1 did not influence the formation of a spike

covering two-to-three blade pitches. The computation should be repeated with more than six blade passages (say eight to twelve) to ensure that the same spike disturbance is obtained.

A primary issue in this work is the general applicability of the proposed criteria for spike formation for any multi-stage compressor. The criteria were obtained from computations and analysis performed with one numerical code and on one isolated rotor geometry with uniform inlet flow. The criterion regarding the incoming/tip clearance flow interface is shown to be generic among other geometries exhibiting spike stall inception and codes, and with inlet stagnation pressure distortion (section 2.3.1). However, the other criterion concerning tip clearance backflow has yet to be rigorously verified on other rotor geometries exhibiting spike disturbances. In addition, the effects of unsteadiness and inlet distortions from adjacent blade rows on both criteria have not been assessed. This issue can be resolved on two fronts.

The first front is experimental validation of the flow criteria on multi-stage compressors that can be made to exhibit both spike and modal stall inception. The procedure consists of determining of the location of incoming/tip clearance flow interface and presence of trailing edge backflow for cases of spike and modal stall inception. The goal is to verify that both leading edge flow spillage and trailing edge backflow below the blade tip are present for spike stall inception and not for modal stall inception.

The second front is computational. Numerical simulations provide an easier quantitative assessment of the leading edge flow spillage and trailing edge backflow than experiments. Here are the sets of tasks that can be done with computations:

(1) Verify the generic nature of the proposed criteria for spike formation with respect to other rotor geometries and CFD codes. This can be accomplished by performing the following computations, operating point by operating point, up to and beyond the last equilibrium solution:

- Time-accurate single blade passage computation on the E3 rotor using a different code

- Time-accurate single blade passage computation on other compressor rotor geometries (both high-speed and low-speed) where spikes disturbances are experimentally shown to originate, using either the present code or a different code. Rotor geometries associated with spikes but also exhibiting suction side blade boundary layer separation near the blade tip should be examined to see the role of blade boundary layer separation on spike formation.

The computations should be examined to assess whether tip blockage growth until reaching the hub characterizes the equilibrium flow limit and if the equilibrium solution limit marks the onset of trailing edge tip clearance backflow (negative mass flow across the pitch) below the blade tip and leading edge tip clearance flow spillage below the blade tip.

(2) Determine the effects of introduced unsteadiness from upstream stator wakes and neighboring stator potential fields on the proposed spike formation criteria by repeating the analysis outlined in point (1) for the rotor in the following computations, performed operating point by operating point up to and beyond the equilibrium solution limit:

- Time-accurate stator-rotor computations (with matched and mismatched blade numbers) using a sliding plane interface to transfer the wake and potential effect from the upstream stator to the rotor

- Time-accurate rotor-stator computations (with matched and mismatched blade numbers) using a sliding plane interface to transfer the potential effect from the downstream stator to the rotor

A secondary recommendation is determination of whether the source of the unsteadiness associated with large tip clearances near the stall point is linked to the tip clearance backflow below the blade tip (appendix D). The goal is to assess whether this unsteadiness can be used to enhance mixing between the tip clearance flow with the core flow to improve compressor performance.

Bibliography

[1] Baldwin, B.S. and Lomax, H., "Thin Layer Approximation and Algebraic Model for Separated Turbulent Flows", AIAA Paper No. 78-257, 1978.

[2] Camp, T.R. and Day, I.J., "A Study of Spike and Modal Stall Phenomena in a Low-Speed Axial Compressor", ASME Journal of Turbomachinery, Vol. 120, pp.393-401, July 1998.

[3] Chen, G.T., Greitzer, E.M., Tan, C.S. and Marble, F.E., "Similarity Analysis of Compressor Tip Clearance Flow Structure", ASME Journal of Turbomachinery, Vol. 113, pp.260-271, April 1991.

[4] Day, I.J., "Stall Inception in Axial Flow Compressors", ASME Journal of Turbomachinery, Vol. 115, pp.1-9, January 1993.

[5] Day, I.J. and Freeman, C., "The Unstable Behavior of Low and High Speed Compressors", ASME Journal of Turbomachinery, Vol. 116, pp.194-201, April 1994.

[6] Dawes,W.N., "The Applications of Mutligrid to Navier-Stokes Simulation of 3D Flow in Axial and Radial Flow Turbomachinery", International Journal for Mumerical Methods, Fluids, Vol. 8, pp.1217-1227, 1988.

[7] Denton, J.D., "The Use of a Distributed Body Force to Simulate Viscous Effects in 3D Flow Calculations", ASME Paper No. 86-GT-144, 1986.

[8] Dobat, A. and Saathoff, H., "Experimentelle Untersuchungen zur Entstehung von Rotating Stall in Axialventilatoren", VDI-Berichte, February 2001.

[9] Furukawa, M., Inoue, M., Saiki, K. and Yamada, K., "The Role of Tip Leakage Vortex Breakdown in Compressor Rotor Aerodynamics", ASME Journal of Turbomachinery, Vol. 121, pp.469-480, July 1999.

[10] Furukawa, M., Saiki, K., Yamada, K. and Inoue, M., "The Role of Tip Leakage Vortex Breakdown in Compressor Rotor Aerodynamics", ASME Paper 2000-GT-666, 2000.

[11] Gong, Y., Tan, C.S., Gordon, K.A. and Greitzer, E.M., "A Computational Model for Short Wavelength Stall Inception and Development in Multi-Stage Compressors", ASME Journal of Turbomachinery, Vol. 121, pp.726-734, October1999.

[12] Greitzer, E.M., " Surge and Rotating Stall in Axial Flow Compressors, Parts I and II", Journal of Engineering For Power, Vol. 98, No. 2 , pp.190-217, April 1976.

[13] Hah, C., Schulze, R., Wagner, S., Hennecke, D.K., "Numerical and Experimental Study for Short Wavelength Stall Inception in a Low-Speed Axial Compressor", Paper AIAA 99-IS-033, 1999.

[14] Haynes, J.M., Hendricks. G.J., and Epstein, A.H., "Active Stabilization of Rotating Stall in a Three-Stage Axial Compressor", ASME Journal of Turbomachinery, Vol. 116, No. 2, pp.226-239, April 1994.

[15] Hoying, D.A., Tan, C.S., Vo, H.D. and Greitzer, E.M., "Role of Blade Passage Flow Structures in Axial Compressor Rotating Stall Inception", ASME Journal of Turbomachinery, Vol. 121, No. 4, pp.735-742, 1999.

[16] Jackson, A.D., "Stall Cell Development in Axial Compressor", ASME Paper 86-GT-249, 1986.

[17] Khalid, S.A., Khalsa, A.S., Waitz, I.A., Tan, C.S., Greitzer, E.M., Cumpsty, N.A., Adamczyk, J.J. and Marble, F.E., "Endwall Blockage in Axial Compressors", ASME Journal of Turbomachinery, Vol. 121, pp.499-509, July 1999.

[18] Koch , C.C., "Discussion of Benser WA: Transonic Compressor Technology Advancements", Fluid Mechanics, Acoustics, and Design of Turbomachinery, Part II, NASA SP-304, 1974.

[19] Koch, C.C., "Stalling Pressure Rise Capability of Axial Flow Compressor Stages", ASME Journal of Turbomachinery, Vol. 103, pp.645-656, 1981.

[20] Lee, N.K.W. and Greitzer, E.M., "Effects of Endwall Suction and Blowing on Axial Compressor Stability Enhancement", ASME Journal of Turbomachinery, Vol. 112, pp.133-144, January 1990.

[21] Mailach, R., Lehmann, I. and Vogeler, K., "Rotating Instabilities in an Axial Compressor Originating From The Fluctuating Blade Tip Vortex", ASME Paper 2000-GT-506, 2000.

[22] Marz, J., Hah, C. and Neise, W., "An Experimental and Numerical Investigation Into the Mechanisms of Rotating Instability", ASME Paper 2001-GT-536, 2001.

[23] Moore, F.K., and Greitzer, E.M., "A Theory of Post-Stall Transients in Axial Compressors, Part I - Development of Equations", ASME Journal of Engineering for Gas Turbines and Power, Vol. 108, pp.68-76, 1986.

[24] Paduano, J.D., "Active Control of Rotating Stall in Axial Compressors", GTL Report No. 208, Massachusetts Institute of Technology, June 1993.

[25] Park, H.G., "Unsteady Disturbance Structures in Axial Flow Compressor Stall Inception", M.S. Thesis, MIT Department of Aeronautics and Astronautics, May 1994.

[26] Saathoff , H. and Stark, U., "Tip clearance Flow Induced Endwall Boundary Layer Separation in a Single-Stage Axial-Flow Low-Speed Compressor", ASME Paper 2000-GT-0501, 2000.

[27] Silkowski, P.D., 1995, "Measurements of Rotor Stalling in a Matched and Mismatched Multistage Compressor", GTL report No. 221, Massachusetts Institute of Technology, April 1995.

[28] Spakovszky, Z.S., Weigl, H.J., Paduano, J.D., Van Schalkwyk, C.M., Suder, K.L. and Bright, M.M., "Rotating Stall Control in a High-Speed Stage with Inlet Distortion: Part I- Radial Distortion", ASME Journal of Turbomachinery, Vol. 121, pp.510-516, July 1999.

[29] Storer, J.A. and Cumpsty, N.A., "Tip Leakage Flow in Axial Compressors", ASME Journal of Turbomachinery, Vol. 113, pp.252-259, April 1991.

[30] Van Zante, D.E., "Rotor 35 LDV Data", NASA Glenn Research Center, December 1999.

[31] Wisler, D.C., "Core Compressor Exit Stage Study", Volume IV- Data and Performance Report for the Best Stage Configuration, NASA CR-165357, NASA LEWIS Research Center,1981.

Appendix A

Assessment of Vortex Kinematics Stall Criteria

Hoying *et al.* [15] suggested a kinematic argument for tip clearance flow instability based on the tip clearance vortex lining up with the leading edge plane. The argument is based on the fact that the tip clearance vortex position is a balance between the component of the incoming velocity normal to the vortex and the induced velocity from the image of the vortex across the casing. Figure A.1a shows that when the tip vortex reaches the leading edge, the (restoring) component of the incoming velocity normal to the vortex is reduced when the vortex is disturbed forward. The vortex would thus tend to move forward and the vortex position is thus unstable.

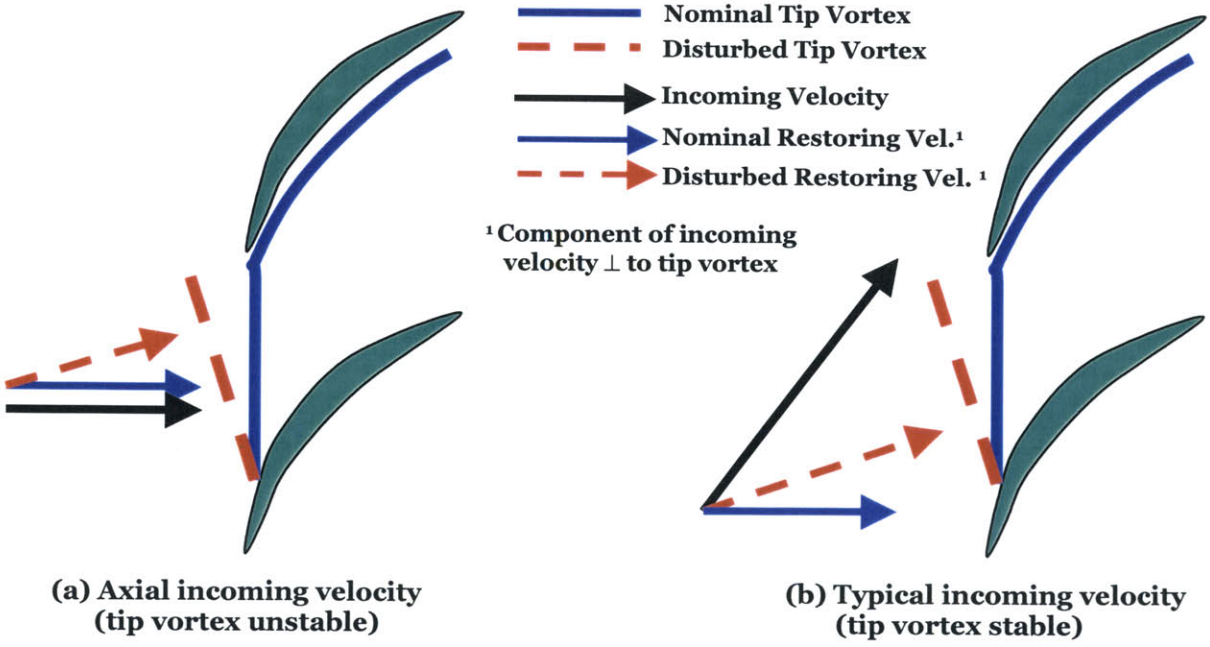

Figure A.1. Tip clearance flow stability argument based on vortex kinematics

However, the above arguments breaks down if the relative incoming flow velocity is not axial, as is the case for compressor rotors, as shown in figure A.1b, where the (restoring) component of the incoming velocity normal to the disturbed vortex is increased and thus the vortex position at the leading edge plane should be stable.

Appendix B

Steady-State Computations

In this appendix, code, mesh and computational procedure for the single blade passage steady-state computations shown in section 2.2 are presented.

B.1 Numerical Code

As mentioned in chapter 2, the code selected for this part of the study is BTOB3D. It is a relatively simple structured Navier-Stokes code written by W. N. Dawes of Cambridge University. It has been used in industry and can capture the tip leakage flow and boundary layer characteristics. This code has a cell-centered scheme and uses the Baldwin-Lomax turbulence model [1] along with wall functions near the solid surfaces to capture the turbulent boundary layer characteristic of compressor blades. Written for 1980s computer technology, the code provides good solutions with coarse meshes. In addition, BTOB3D possesses two useful characteristics suited for this study.

First, it provides relatively good convergence speed (on the order of a day), which is needed considering the number of speedlines that were run for section 2.2. This requirement becomes even more important the equilibrium flow limit is approached on each speedline, where convergence time has been observed to increase several fold.

Second, the source code was provided, allowing us to modify the code to compute and output the flow properties that are important to this problem.

A more detailed description of BTOB3D can be found in reference [6].

B.2 Mesh

The computational grid used for the steady-state single blade passage computations on the E3 rotor B contains 53,505 nodes, with 45, 29 and 41 nodes in the axial, pitch and radial directions, respectively. Figure B.1 shows the grid for the blade, hub, axial and pitch surfaces. The inlet boundary is placed one axial chord length (or 0.75 pitch) upstream of the blade leading edge to minimize the effect of the axisymmetric inlet boundary conditions on the blade flow field by allowing disturbances with wavelength on the order of the blade pitch to decay over the length of the upstream duct. Similarly, the downstream blade duct is placed at 2.7 times axial chord length (1.9 pitch) downstream of the blade trailing edge. The extra duct length allows the tip clearance flow to mix out and avoid negative axial velocity at the exit boundary condition which the code was not designed to handle.

Figure B.1 also shows that the radial grid spacing near the end walls is coarse at the domain inlet plane and becomes finer toward the blade leading edge plane. This feature was necessary for the code to work properly with a finer radial grid in the blade tip clearance region. The side effect was to make the incoming casing boundary layer at the blade leading edge insignificant for a uniform inlet stagnation pressure distribution. Previous single blade passage computations with the code used by Hoying [15] suggest that the presence of an incoming casing boundary layer only shifts the equilibrium flow limit to a higher flow coefficient without modifying the flow features in the tip region. Thus, the presence of an inlet boundary layer boundary layer is not judged to be crucial at this stage in the study of spike stall inception.

In addition, the simplicity of the BTOB3D mesh requires that the blade have a pinched tip (zero thickness), as depicted in figure B.2. Storer *et al.* [29] found that the tip clearance flow is mainly pressure driven. Therefore, the tip clearance flow through a pinched tip should behave in a similar manner to that through a square tip, if only with a different effective tip clearance.

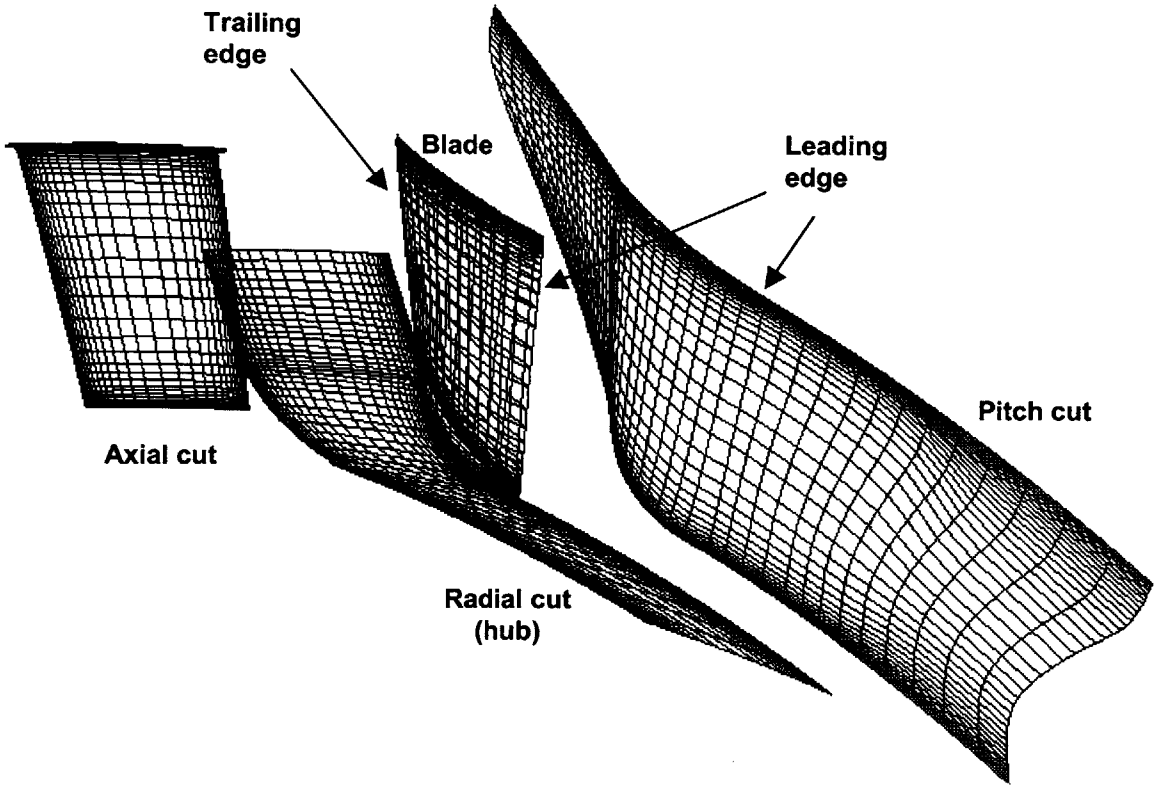

Figure B.1. BTOB3D mesh of E3 Rotor B blade passage geometry

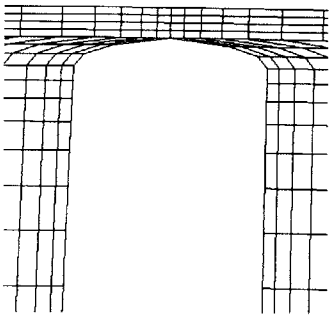

Figure B.2. BTOB3D mesh of blade tip (axial cut)

In summary, the mesh used for this part of the study is relatively coarse but is judged to be adequate at this early this stage of the study to identify flow features associated with spike stall inception.

B.3 Computational Procedure

The boundary conditions prescribed in BTOB3D are:

- Domain inlet: Uniform stagnation pressure and temperature at atmospheric value and axisymmetric radial distribution of swirl angle based on the spanwise distribution of the inlet guide vanes' exit angle.

- Domain exit: Axisymmetric static pressure at tip with radial equilibrium. This back pressure was usually constant for a particular run. However, for large tip clearance sizes such as is the case described in section 2.2.2, where exit pressure turn over was present (figure 2.5), a simple throttle was added to the code where the exit tip back pressure was a function of the mass flow through the domain. The goal was to try to get as far below (in terms of mass flow) the pressure rise turnover point as possible.

- Surfaces: All surfaces are viscous, so as to include boundary layer separation as a possible cause of stall. The blade boundary layer is assumed to be turbulent from the blade leading edge plane. This is a reasonable assumption for compressor blades since the fluid flows against a pressure gradient, thus transition from laminar to turbulent should occur very close to the leading edge

- Rotating speed: Scaled up 2.5 times to give a tip Mach number of 0.5 to reduce convergence time yet still have minimal compressibility effects.

The first step consists of getting an initial equilibrium flow solution using a low back pressure and starting the computation from a crude initial flow field set up by BTOB3D with the given boundary conditions. Using the obtained initial equilibrium solution, one moves up the pressure rise characteristics by increasing the prescribed tip back pressure in steps of 300 Pa (0.17 times the dynamic head based on rotor tip speed), until the an

equilibrium flow solution no longer exists. Convergence history for prescribed back pressure beyond the equilibrium solution limit was characterized by an exponential drop in the mass flow through the rotor and an accompanying growth in the residual. Using the equilibrium solution with the lowest mass flow as the new initial condition, the previous procedure is repeated in increasingly smaller increments of tip back pressure until one gets the equilibrium solution limit to within one Pa.

Appendix C

Unsteady (Time-Accurate) Computations

This appendix gives more detail on the code, mesh and computational procedure used in the time-accurate single and multiple blade passage computations described in chapter 3 and 4.

C.1 Numerical Code

As mentioned in chapter 3, the time-accurate code used in this study is UNSTREST, written by J. D. Denton of Cambridge University. It has a similar input data structure to BTOB3D and has also been widely used. However, unlike BTOB3D, UNSTREST uses a simple mixing length turbulence model. The mixing length is input for each blade row. A value of 0.05 times the mid span pitch, extracted from the steady computations with BTOB3D, was used in this case. It must be noted that the exact value is not important as we looking for trends and not exact performance predictions. UNSTREST can handle multiple blade passages, a feature needed for the stall inception simulations described in chapter 4. It is also faster than BTOB3D, thus allowing us to increase the mesh size to better capture the passage flow features identified in chapter 2 without significantly increasing computation time. Reference [7] provides more information on UNSTREST.

C.2 Mesh

Due to the simpler turbulence model, UNSTREST is at least twice faster than BTOB3D for the same grid size. Thus, a finer mesh can be used that put more axial grid points to better resolve the blade leading edge region where the incoming/tip clearance flow interface lies for rotors exhibiting spike stall inception (chapter 2). A refined mesh obtained from the previous mesh used with BTOB3D (figures B.1 and B.2) was proposed by Denton and is shown in figures C.1 and C.2.

Comparing this mesh with that used in BTOB3D (figure B.1), one first sees that the mesh is finer (106 x 41 x 45 compared to 45 x 29 x 41) in both the axial and pitchwise directions.

Second, the pinched blade tip (figure C.2) is much more pointed than in the previous mesh (figure B.2). However, since the tip clearance flow is primarily a pressure driven flow [29], the only effect of the pointed tip is to change the effective tip clearance size without changing the trend.

Third, the upstream and downstream ducts are much longer so that the single blade passage mesh can be repeated to make a multiple blade passage mesh. The length of the upstream and downstream ducts must equal the width of the multiple blade computational domain such that any disturbance with a wavelength on the order of the domain width can decay to uniform conditions in the pitchwise direction at the boundaries, as required by the code. Thus, to keep the axial and total circumferential grid sizes down so that the computational time remains reasonable, the number of blade passages simulated must be kept at a minimal without affecting the physics of the problem. Since a spike has been experimentally measured to have a pitchwise extent of two to three blade pitches, it is judged that six blade passages are sufficient to simulate spike stall inception. Thus, the ducts are about six blade pitches in length. The total number of nodes is thus 1,173,420 and one rotor revolution requires about 77 hours on a personal computer with an AMD Atlon 1.2 GHz processor. Since an actual spike grows to full stall in three to five iterations, a spike stall inception simulation should last on the order of a few weeks.

Finally, unlike the mesh used in BTOB3D, there is very little change in radial grid spacing from the domain inlet to the blade leading edge, such that the endwall radial grid

spacing remains fine along the entire duct. The large incoming casing and hub boundary layer that would have resulted from the long duct is avoided by a modification in the code to make the duct's endwall inviscid almost until the blade leading edge plane.

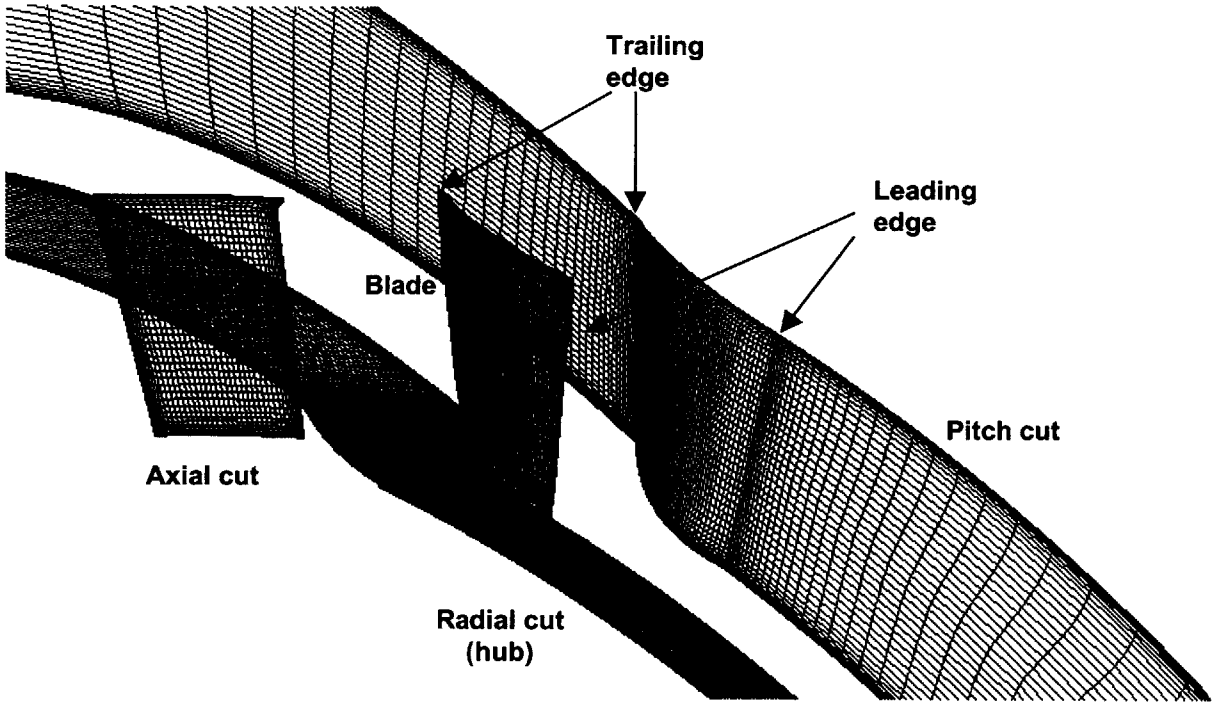

Figure C.1. UNSTREST mesh of the E3 rotor B blade passage geometry

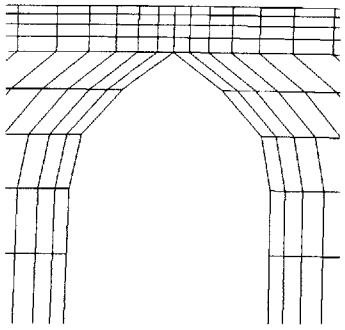

Figure C.2. UNSTREST mesh of blade tip (axial cut)

C.3 Computational Procedure

The computational procedure to obtain the speedlines up to the equilibrium solution limit, as shown in figure 3.2, is the same as described for steady computations in section B.3.

To initiate the stall flow transient, the equilibrium flow limit is used as the initial solution, the back pressure exit boundary conditions is increased slightly, in this case by about 15 Pa or 0.08% of the dynamic head based on blade tip speed. This procedure is the same for multiple blade passage stall simulation, except that the single blade passage solution limit and mesh is repeated six times circumferentially as shown in figure C.3.

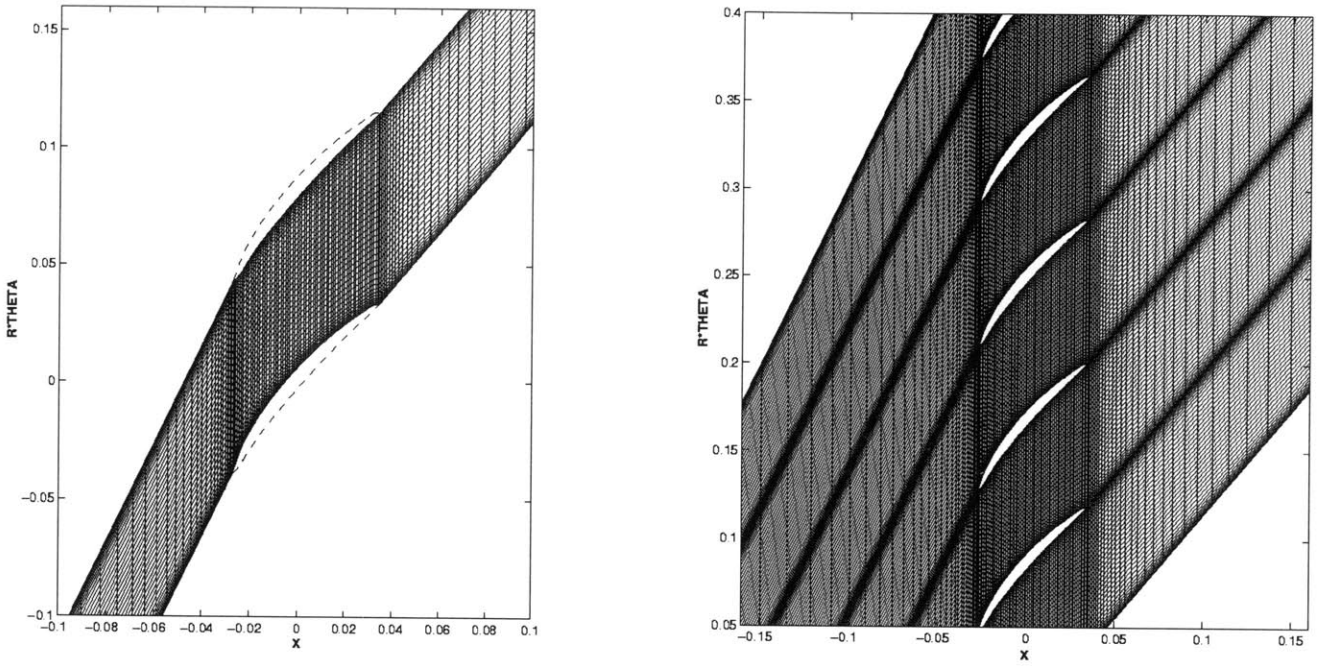

Figure C.3. Single and multiple blade passage meshes

However, UNSTREST solves the flow in cylindrical coordinates and thus leaves no room for any asymmetry introduced by truncation errors that would occur if the compressor's cylindrical geometry were resolved in Cartesian coordinates. Thus, without the introduction of asymmetry in the flow field, the multiple blade passage stall transient would occur simultaneously for every blade passage. Consequently, it is necessary to introduce an asymmetry in the flow field without prejudicing the results in favor of spikes. The chosen method consists of applying a temporary full-span (radially uniform) stagnation pressure disturbance at the domain inlet plane with a circumferential wavelength of six blade passages, rotating with the blades. This should favor modal stall inception should it occur. The inlet disturbance amplitude was selected to give about 100 Pa (0.5% of the dynamic head based on blade tip speed) in stagnation pressure disturbance amplitude at the blade leading edge. This value is on the order of magnitude

of the increase in back pressure beyond the equilibrium flow limit. The application time is ten blade passing times, or about 1/6 or a rotor revolution, which is small with respect to the development time of a spike into a stall cell (3 to 5 rotor revolutions).

Appendix D

Flow Oscillations at Large Tip Clearances

In Chapter 3, steady oscillations concentrated in the tip region flow field were observed for tip clearances above 1.8% chord. The amplitudes of the oscillations increased with tip clearance size and with decreasing flow coefficient. Figure 3.2 shows that for the 3.0% chord tip clearance case the amplitudes of the oscillations are very significant (over 10% of the compressor total-to-static pressure rise). In this appendix, a frequency analysis of these oscillations is carried out in the hope of finding their source.

Figure D.1 shows the power spectral density (PSD) of the oscillations in mass flow at different time-averaged flow coefficients (*Vx/Utip*) for the points shown in figure 3.2 in the 3.0% chord tip clearance configuration. One can see that there is a dominant oscillation at the frequency around 0.4 times the blade passing frequency (based on the blade passing time over one pitch). The amplitude of this oscillation increases rapidly with decreasing flow coefficient. Its frequency decreases with decreasing flow coefficient (i.e. increased flow convection time across the passage). In addition, for flow coefficients between 0.41 and 0.44, lower amplitude oscillations with fixed frequencies at 0.06, 0.16 and 0.2 times the blade passing frequency are also visible whose amplitudes do not follow any particular trend.

To verify if these frequencies are linked to acoustic resonances, the length of the computational domain was varied by changing the length of the ducts upstream and downstream of the blade passage. In order to keep the computational mesh size reasonable, the number of axial nodes in the ducts was not changed. Thus, only modest changes in duct length of up to 30% could be achieved without stretching the grid too far.

The PSD analysis with respect to domain length ratio is shown in figure D.2. Since none of the frequencies are affected by the length of the computational domain, acoustic resonance can be ruled out as a source.

The lack of any trends for the small frequencies implies that they have numerical rather than physical origins. This could be investigated by changing the grid size both outside and inside the blade passage.

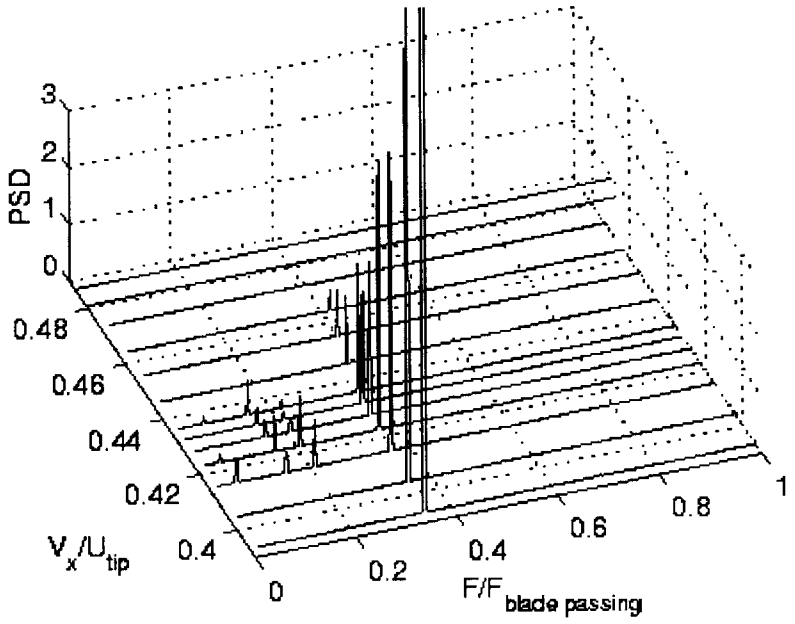

Figure D.1. PSD analysis for 3.0% chord tip clearance at different flow coefficients

On the other hand, the dominating oscillation is highly suspected to be physical since its frequency and amplitude follow a definite trend in terms of flow coefficient. In addition, it arises only at larger tip clearances as observed experimentally by Mailach *et al.* [21] in their observations of tip clearance oscillations, and its frequency (~0.37 of rotor blade passing frequency) is in the same range as the rotating instability frequencies measured by Mailach *et al.* [21] (~0.23) and Marz *et al.* [22] (~0.29). In section 3.2, the tendency of impinging backflow below the blade tip to propagate towards the leading edge was discussed. However, it cannot do so when the incoming/tip clearance flow is inside the blade passage as is the case for the equilibrium solution range for tip clearance sizes above 1.8% chord. Since it is in this range of tip clearance size that tip clearance

flow oscillations were observed, it is suspected that the source of these oscillations is linked to the impinging backflow trying to propagate toward the leading edge while being held back by the incoming flow. However, this conjecture needs further investigation.

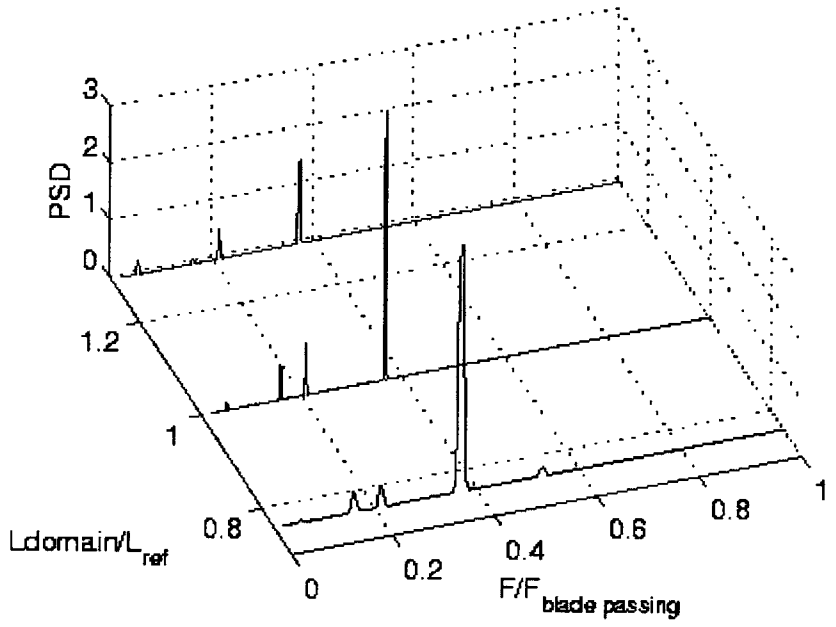

Figure D.2. Effect of domain length on oscillation frequencies